

The interaction of p130Cas with PKN3 promotes malignant growth

Jakub Gemperle, Michal Dibus, Lenka Koudelková, Daniel Rosel and Jan Brábek 

Department of Cell Biology, Faculty of Science – Biocev, Charles University, Prague 2, Czech Republic

Keywords

BCAR1; CAS; p130Cas; PKN3; SH3; Src

Correspondence

J. Brábek, Department of Cell Biology,
Faculty of Science – Biocev, Charles
University, Vinicna 7, 12843 Prague 2,
Czech Republic
Tel: +420 32587 3900
E-mail: jan.brabek@natur.cuni.cz

(Received 17 July 2018, revised 5 October
2018, accepted 28 October 2018, available
online 3 December 2018)

doi:10.1002/1878-0261.12401

Protein p130Cas constitutes an adaptor protein mainly involved in integrin signaling downstream of Src kinase. Owing to its modular structure, p130Cas acts as a general regulator of cancer cell growth and invasiveness induced by different oncogenes. However, other mechanisms of p130Cas signaling leading to malignant progression are poorly understood. Here, we show a novel interaction of p130Cas with Ser/Thr kinase PKN3, which is implicated in prostate and breast cancer growth downstream of phosphoinositide 3-kinase. This direct interaction is mediated by the p130Cas SH3 domain and the centrally located PKN3 polyproline sequence. PKN3 is the first identified Ser/Thr kinase to bind and phosphorylate p130Cas and to colocalize with p130Cas in cell structures that have a pro-invasive function. Moreover, the PKN3–p130Cas interaction is important for mouse embryonic fibroblast growth and invasiveness independent of Src transformation, indicating a mechanism distinct from that previously characterized for p130Cas. Together, our results suggest that the PKN3–p130Cas complex represents an attractive therapeutic target in late-stage malignancies.

1. Introduction

p130Cas (Crk-associated substrate, CAS; BCAR1) is a molecular scaffold involved in the regulation of several processes, such as actin cytoskeleton remodeling, cell survival, migration, invasion, and proliferation in both normal and pathological cells (Cabodi *et al.*, 2010a; Tikhmyanova *et al.*, 2010). Owing to its modular structure, p130Cas plays a crucial role in signaling originating from many mutated or amplified oncogenes (Nikonova *et al.*, 2014; Tikhmyanova *et al.*, 2010; Tornillo *et al.*, 2014). It has been reported that knock-down of p130Cas leads to proliferative arrest in breast cancer cell lines carrying oncogenic mutations in *BRAF*, *KRAS*, *PTEN*, or *PIK3CA* (Pylayeva *et al.*,

2009). Moreover, its involvement in Src-mediated tumorigenesis has been clearly demonstrated. For example, Src-transformed mouse embryonic fibroblasts (MEFs) exhibit increased ability to invade through Matrigel and induce metastases in mice in a p130Cas-dependent manner (Brábek *et al.*, 2004, 2005; Honda *et al.*, 1998). Other studies *in vivo* have shown that p130Cas also drives the growth, aggressiveness, and progression of ErbB2-overexpressing breast tumors, including metastatic colonization of the lungs (Cabodi *et al.*, 2006, 2010b). Correspondingly, elevated expression of p130Cas in human patients is associated with early disease recurrence and poor prognosis in several cancer types, including lung, prostate, pancreas, ovarian, and mammary cancers (Cabodi *et al.*, 2010a;

Abbreviations

BCAR1, breast cancer anti-estrogen resistance protein 1; CCH, CAS-family C-terminal homology domain; DMEM, Dulbecco's modified Eagle's medium; Dox, doxycycline; ECM, extracellular matrix; FN, fibronectin; KO, knockout; MDApkn3^{-/-}, MDA-MB-231 pkn3^{-/-}; MEF, mouse embryonic fibroblast; mPR, mutation P₅₀₀PPKPPRL to PAPSAPRL (mouse PKN3 mutant unable to bind p130Cas); p130Cas, Crk-associated substrate (size 130 kDa); PI3K, phosphoinositide 3-kinase; PKN3, protein kinase N3; RTCA, real-time cell analysis; SC, p130Cas^{-/-}; MEFs re-expressing p130Cas transformed by SrcF; SCpkn3^{-/-}, SC PKN3 KO; SrcF, constitutively active Src (Src Y527F); SRD, serine-rich domain.

Defilippi *et al.*, 2006; Fromont and Cussenot, 2011; Fromont *et al.*, 2007; Nick *et al.*, 2011; Nikonova *et al.*, 2014; Tikhmyanova *et al.*, 2010) and is associated with hormone deprivation-mediated resistance to antitumor drugs (standard therapeutics) such as adriamycin (doxorubicin) and tamoxifen (Dorssers *et al.*, 2001; Ta *et al.*, 2008). Taken together, such evidence clearly underlines a role for p130Cas as a general regulator of cancer cell growth and metastasis as induced by different oncogenes.

The structure of p130Cas consists of an N-terminal SRC homology 3 (SH3) domain, substrate domain (SD), and serine-rich domain (SRD) followed by Src and phosphoinositide 3-kinase (PI3K) binding regions and terminated by a CAS-family C-terminal homology domain (CCH) (Cabodi *et al.*, 2010a). The majority of known p130Cas downstream signaling is attributed to tyrosine phosphorylation of a repeated YXXP motif within the p130Cas SD domain (Cabodi *et al.*, 2010a; Defilippi *et al.*, 2006). The level of p130Cas tyrosine phosphorylation is mainly dependent on the binding capacity of its SH3 domain, which facilitates direct interaction of p130Cas with the polyproline motif of various phosphatases (e.g., PTP1B, PTP-PEST) and kinases (FAK, PYK2) or mediates indirect association with Src via a FAK (PYK2) bridge (Astier *et al.*, 1997; Fonseca *et al.*, 2004; Ruest *et al.*, 2001). Specifically, association of p130Cas via the p130Cas SH3 domain with FAK and Src at focal adhesions transmits signals that induce lamellipodia and cell migration, support cell proliferation and cell invasiveness, and block anoikis (Brábek *et al.*, 2005; Defilippi *et al.*, 2006; Donato *et al.*, 2010; Nikonova *et al.*, 2014; Ruest *et al.*, 2001; Tazaki *et al.*, 2008). p130Cas has also been shown to be phosphorylated at serine residues, which can be induced by protein BCAR3 and is partially dependent on the p130Cas SH3 domain; however, responsible serine/threonine kinases have not yet been identified (Makkinje *et al.*, 2009). In addition, p130Cas has been shown to interact with 14-3-3 proteins in a phosphoserine-dependent manner, which occurs mainly at lamellipodia during integrin-mediated cell attachment to the extracellular matrix (ECM; Garcia-Guzman *et al.*, 1999).

In a screen for new interaction partners of the p130Cas SH3 domain, we recently predicted a list of candidates and verified p130Cas SH3 binding to the polyproline motifs of GLIS2 and DOK7 (Gemperle *et al.*, 2017). Among other predicted candidates, serine/threonine PKN3 kinase, with the polyproline motif P₅₀₀PPKPPRL, constitutes a member of the PKN family, which is part of the protein kinase C (PKC)

superfamily of serine/threonine kinases. The role of PKN3 in tumorigenesis was identified in early reports, which showed that *PKN3* mRNA is scarce in normal human adult tissues but abundantly expressed in numerous cancer cell lines (Oishi *et al.*, 1999). In contrast, the other members of the PKN family, PKN1 and PKN2, exhibit ubiquitous expression in human and rat tissues (Hashimoto *et al.*, 1998; Mukai and Ono, 1994; Quilliam *et al.*, 1996). PKN3, but not PKN1 or PKN2, has been shown to regulate malignant prostate cell growth downstream of activated PI3K independent of Akt (Leenders *et al.*, 2004), and moreover, only PKN3 possess the polyproline sequence in its central portion that we have predicted as a potential p130Cas SH3 domain binding site (Gemperle *et al.*, 2017). In addition, when stimulated in a fatty acid-dependent manner, the catalytic activity of PKN3 was less responsive in comparison to PKN1 and PKN2, thereby highlighting the differences in function of PKN isoforms, as well as their regulation (Oishi *et al.*, 1999).

Using orthotopic mouse tumor models, the effect of PKN3 on cancer growth was shown by conditional reduction of PKN3 expression in tumors. In all cases, downregulation of PKN3 protein impaired primary prostate and breast tumor growth and blocked metastasis (Aleku *et al.*, 2008; Leenders *et al.*, 2004; Unsal-Kacmaz *et al.*, 2012). Correspondingly, overexpression of exogenous PKN3 in breast cancer cells further increased their malignant behavior *in vitro* (Unsal-Kacmaz *et al.*, 2012). Although PKN3 KO mice appeared indistinguishable from their WT counterparts, this model also indicated the role of host stromal PKN3 in tumor progression (Mukai *et al.*, 2016). Stromal PKN3 is enriched in primary endothelial cells as well as in osteoclasts (Uehara *et al.*, 2017), being apart from tumor cells among the few normal cell types with significant amount of PKN3; this is consistent with the usually invasive features of endothelial cells in particular (Aleku *et al.*, 2008). Accordingly, systemic administration of siRNA-lipoplex (Atu027) directed against PKN3 and targeting mainly the stromal compartment rather than the pathologically defined tumor entity, prevented lung metastasis in lung experimental and spontaneous breast metastasis models in a dose-dependent manner (Santel *et al.*, 2010).

In mammalian tissues, the PKN family underlies some of the main Rho GTPase-associated protein kinase activities (Lim *et al.*, 2008; Mellor *et al.*, 1998; Vincent and Settleman, 1997). Specifically, Unsal-Kacmaz *et al.* (2012) demonstrated that PKN3 physically interacts with Rho-family GTPases, and preferentially

with RhoC, a known mediator of tumor invasion and metastasis in epithelial cancers. However, additional molecular mechanisms by which PKN3 contributes to malignant growth and tumorigenesis are not well understood.

In this study, we have shown that PKN3 directly interacts with p130Cas and phosphorylates it *in vitro* and potentially *in vivo*. Furthermore, we have demonstrated the importance of the PKN3–p130Cas interaction for PKN3-stimulated cell growth and invasiveness *in vitro* and tumor growth *in vivo*.

2. Materials and methods

2.1. Antibodies and reagents

The following antibodies were used: Akt (rabbit pAb, #9272S), phospho-Akt (Ser473, rabbit mAb D9E, #4060S), phospho-p130Cas (Tyr165, rabbit pAb), p44/42 MAPK (i.e., Erk1/2, rabbit mAb 137F5, #4695), phospho-Src family (Tyr416, rabbit pAb, #2101S), Stat3 (rabbit mAb D3Z2G, #12640), Phospho-Stat3 (Tyr705, mouse mAb 3E2, #9138S), Phospho-Myosin Light Chain 2 (Ser19, mouse mAb, #3675), Phospho-S6 Ribosomal Protein (Ser235/236, rabbit mAb 2F9, #4856), S6 Ribosomal Protein (rabbit mAb 54D2, #2317), Phospho-GSK-3 α/β (Ser21/9, Rabbit mAb 37F11, #9327), Phospho-p130Cas (Tyr165, rabbit pAb, #4015; Cell Signaling Technology, Danvers, MA, USA); Phospho-FAK (Tyr397, rabbit pAb, #44-624G; Thermo Fisher Scientific, Waltham, MA, USA); p130Cas (mouse mAb 24), Paxillin (mAb 349; BD Biosciences, San Jose, CA, USA); Src (mouse mAb 327, Ab-1; Calbiochem, San Diego, CA, USA); FAK (rabbit pAb, C-20), Actin (goat pAb, C-11; Santa Cruz Biotechnology, Dallas, TX, USA); MAPK (i.e., Erk1/2, mouse mAb V114A; Promega, Madison, WI, USA); GST (rabbit pAb, G7781; Sigma-Aldrich s.r.o., St. Louis, MO, USA); PKN3 (rabbit pAb, NBP-130102 for detection of human PKN3), mCherry (rabbit pAb, NBP2-25157), StrepII (mAb 517, NBP2-43735; NOVUS Biologicals, Littleton, CO, USA); PKN3 (rabbit pAb, AP14628A for detection of mouse PKN3; Abgent, San Diego, CA, USA); and phospho-PKN3 (human Thr860 = mouse Thr849; Pfizer, Oncology, New York, NY, USA). Immunoprecipitations were carried out using a Flag antibody (mouse mAb M2; Sigma-Aldrich s.r.o.) and GFP antibody (rabbit polyclonal ab290; Abcam, Cambridge, UK). Secondary antibodies fused to HRP (Abcam) were used as recommended by the manufacturer. The secondary antibodies for fluorescence imaging were as follows: anti-rabbit

(Alexa-546) and anti-mouse (Alexa-594, Alexa-633; Thermo Fisher Scientific). The following inhibitors were used (for dilution see Fig. S6A): SB202190, Rapamycin, PF 573228 (Santa Cruz Biotechnology); BIRB796 (Sellckchem, Munich, DEU); Palbociclib, Gefitinib (LC Laboratories, Woburn, MA, USA); DMSO (negative control), ML-7, CI-1040, Latrunculin A (Sigma-Aldrich s.r.o.); Saracatinib (BioVision, Milpitas, CA, USA).

The reagents used were doxycycline hydrochloride, blasticidin, and puromycin (Sigma-Aldrich s.r.o.), glutathione (reduced, LOBA Chemie, Mumbai, India), Phalloidin 405 and FN (Thermo Fisher Scientific), collagen R solution (SERVA Electrophoresis GmbH, Heidelberg, Germany), Matrigel (Corning, Corning, NY, USA), Strep-Tactin[®] Superflow[®] resin (IBA Lifesciences, Göttingen, Germany), nProtein A Sepharose 4 Fast Flow (GE Healthcare, Chicago, IL, USA), anti-Flag M2 affinity resin (Sigma-Aldrich s.r.o.), and *p*-nitrobenzyl mesylate (Abcam).

2.2. Cell lines and culture conditions (shRNA, transfection, retrovirus, and lentivirus preparation)

p130Cas^{-/-} MEFs were obtained from Steven Hanks (Vanderbilt University, Nashville). p130Cas^{-/-} MEFs expressing constitutively active mouse Src Y527F (SrcF cells) or both p130Cas WT and Y527F (SC cells) were prepared using the LZRS-MS-IRES-GFP retroviral vector and the Phoenix E packaging line as described previously (Brábek *et al.*, 2004). Spontaneously immortalized primary fibroblasts (MEFs p130Cas^{-/-}) used in this study were kindly provided by Hisamaru Hirai (Honda *et al.*, 1998). p130Cas^{-/-} MEFs re-expressing p130Cas WT used in this study have very similar p130Cas expression level with that of endogenous p130Cas in normal MEFs (Fonseca *et al.*, 2004).

To generate SC PKN3 null, cells were transiently transfected by sgRNA anti-PKN3 (sequence provided in Table S2) and a puromycin resistance-expressing CRISP-CAS9 plasmid. Cells were selected by puromycin for 2–3 days followed by clonal isolation. Success of CRISPR targeting was analyzed by PCR and Surveyor nuclease assay as published (Ran *et al.*, 2013) and by western blots. Sequences around the CRISPR modification site were amplified by PCR from three selected mammalian clones, cloned into pJET1.2/blunt using a CloneJET PCR Cloning Kit (Thermo Fisher Scientific), and sequenced (at least six from each). Sequencing revealed that CRISPR nicking most frequently caused frameshift –1 bp or +49/+37 bp.

Potential off-targets were predicted (<http://tools.genome-engineering.org>) and the three most potent tested by Surveyor assay (results negative, primer sequences provided in Table S2). SC cells with Dox-inducible PKN3 shRNA (see Plasmid construction, below) were prepared similarly as described previously (Czauderna *et al.*, 2003; Leenders *et al.*, 2004).

MDA-MB-231 cells used for cell transfections were obtained from ECACC (#92020424). All transfections were carried out according to the manufacturer's protocol using Jet Prime (Polyplus Transfection, Illkirch, France) or PEI transfection reagent (Polysciences, Warrington, PA, USA). MDA-MB-231 cells used to generate PKN3 knockout were transfected by sgRNA anti-PKN3 (sequence provided in Table S2), and the puromycin resistance-expressing CRISP-CAS9 plasmid followed by a selection procedure similar to that described above for SC cells. Transfection of siRNA (sequences provided in Table S2; siRNA anti-Luciferase used as control) was carried out according to the manufacturer's protocol using GeneMute (Signagen Laboratories, Rockville, MD, USA).

To stably deliver Flag-fused or mCherry-Flag-fused constructs, retroviral pMSCV-puro or lentiviral pLVX-Tet-On Advanced system (Clontech, Mountain View, CA, USA) was used. In brief, cells were infected with viral supernatant generated in transfected Phoenix E packaging cells (pMSCV system) or produced in HEK293T cells co-transfected by pVSV-G and psPAX2 plasmids together with pLVX-Tet-On in the first round or with pLVX-tight-puro in the second. All cells were then selected with puromycin ($2.5 \mu\text{g}\cdot\text{mL}^{-1}$) or/and blasticidin ($2\text{--}4 \mu\text{g}\cdot\text{mL}^{-1}$) and alternatively sorted by FACS (1–3 rounds) after transient (24 h) induced expression by Dox. Cells without fluorescent protein were cloned and tested by western blot. SCpkn3^{-/-} cells from clone 1 were used for reintroduction of mouse PKN3 and two clones of MDA-MB-231pkn3^{-/-} cells for reintroduction of human PKN3 (mCherry-Flag-fused constructs; similar results). To reintroduce GFP-fused p130Cas variants to p130Cas^{-/-} MEFs, a retroviral pBabe system was used. After infection of p130Cas^{-/-} MEFs by viral supernatants prepared in HEK293T cells co-transfected by pVSV-G, Gag-Pol, and pBabe plasmids, respectively, GFP-positive cells were selected by FACS.

All cells were cultivated in full Dulbecco's modified Eagle's medium (DMEM; Sigma-Aldrich s.r.o.) with $4.5 \text{ g}\cdot\text{L}^{-1}$ L-glucose, L-glutamine, and pyruvate, supplemented with 10% FBS (Sigma-Aldrich s.r.o.) and ciprofloxacin ($0.01 \text{ mg}\cdot\text{mL}^{-1}$) at 37 °C and 5% CO₂. Cells were confirmed as being negative for mycoplasma contamination by PCR.

2.3. Plasmid construction

cDNA coding for p130Cas SRD domain variants (WT, 15AN; sequences provided in Table S1) were commercially synthesized and cloned into the pMA-T vector (geneArt, Thermo Fisher Scientific). The 15AN variant was generated by mutation of all 15 Ser/Thr to Ala or Asn. Mutant variant S432A (KRLS to KRLA) was created subsequently by whole plasmid synthesis using Q5 polymerase (New England Biolabs, Ipswich, MA, USA) and respective site-directed mutagenesis primers (listed in Table S2). Following PCR, 5U of DpnI was added to each reaction and incubated for 1.5 h at 37 °C. Individual mutated clones were screened by sequencing. Sequences of all SRD variants were then switched with the original p130Cas SRD domain cassette within the p130Cas sequence (pUC19 vector) using Bpu10I/SacII sites. pEGFP-C1 p130Cas variants and pGEX-p130Cas-SH3 domain constructs were prepared similarly as described previously (Braniš *et al.*, 2017; Janoštiak *et al.*, 2011). GFP-fused p130Cas variants were introduced into the pBabe retroviral expression vector by EcoRI and blunt end (generated by BamHI/AgeI restriction followed by fill in by Klenow) cloning. All constructs were verified by sequencing. To prepare the GSK3-derived peptide fused to GST, a pair of phosphorylated oligonucleotides (Table S2) was annealed and inserted in frame at the 3' end of the GST (pGEX vector) using BamHI/EcoRI sites. Production of GST-fused proteins (SH3, GSK3) from the pGEX system was carried out as in Gemperle *et al.* (2017). Oligos for sgRNA construction and primers for CRISPR off-target screening were designed and plasmids constructed (Lenti-CRISPR, BsmBI site) as published (Ran *et al.*, 2013) and are listed in Table S2. PKN3 shRNA was cloned into a lentivirus-adapted vector system allowing Dox-inducible expression of shRNA (Czauderna *et al.*, 2003) via PCR followed by ligation and DpnI-mediated cleavage of template DNA. Primers are listed in Table S2. Correct insertion of the shRNA sequence was confirmed first by restriction analysis to confirm the reintroduced BsrGI restriction site and then with DNA sequence analysis.

cDNA coding for whole mouse PKN3 with added sequence for Flag epitope and shorter sequence with mutations to create mPR and KD variants (sequences provided in Table S1) were commercially synthesized and cloned into pMK-RQ or in pMA-T vectors, respectively (geneArt, Thermo Fisher Scientific). The mPR mutant was created to abrogate binding to p130Cas (motif P₅₀₀PPKPPR to PAPSAPR) similarly as suggested in Gemperle *et al.* (2017). The KD

mutation was designed as published for human PKN3 (Leenders *et al.*, 2004). Sequence for mPR was swapped within whole PKN3 in the pMK-RQ vector using NdeI/HindIII sites, and that for KD by NdeI/BamHI followed by cloning PKN3 variants (WT, mPR, KD) to other corresponding vectors: mCherryC1/eGFP C1 (BsrGI/EcoRI), pMSCV-Puro (XhoI/EcoRI), and pLVX-Tight-Puro (BsrGI/EcoRI). A lentiviral expression vector pLVX-Tight-Puro allowing Dox-inducible gene expression was also prepared with mCherry-fused PKN3 variants via NheI/EcoRI and XbaI/EcoRI sites. Flag-fused mCherry control was prepared similarly, except prior to cloning to the pLVX-Tight-Puro system, Flag sequence was inserted in frame in front of mCherry in mCherry C1 vector by annealing the phosphorylated oligonucleotides described in Table S2 and digested NheI/HindIII vector sites. Prior to kinase reactions *in vitro*, Flag-PKN3 was also cloned to the StrepII pcDNA3 vector using blunt end ligation (AfeI/EcoRV vector sites, Flag-PKN3 cleaved from pMSCV-puro by BsrGI/EcoRI and filled in by Klenow). CFP or mCherry-fused LifeAct was prepared as published (Riedl *et al.*, 2008). All constructs were verified first by restriction analysis and then by sequencing.

Plasmid (pcDNA4) coding Flag-fused human PKN3 was a gift from K. Unsal-Kacmaz (Pfizer). This construct was fused in frame to mCherry (mCherryC1 vector modified via PCR; EcoRI/XhoI) and cloned to pLVX-Tight-Puro (NheI/XbaI and MluI).

2.4. Preparation of cell extracts and immunoblotting

Cell were lysed in RIPA (total lysates; composition: 150 mM NaCl; 50 mM Tris/HCl, pH 7.4, 1% Nonidet P-40, 0.1% SDS, 1% sodium deoxycholate, 5 mM EDTA, 50 mM NaF) or in 1% Triton lysis buffer [immunoprecipitations, pull-downs; composition: 50 mM Tris/HCl (pH 7.1), with 150 mM NaCl and 1% Triton X-100] supplemented with protease (MixM) and phosphatase inhibitors (MixII; SERVA Electrophoresis GmbH) followed by immunoblotting as described previously (Janošiak *et al.*, 2014). In brief, protein extracts were separated using SDS/PAGE under denaturing conditions (6–15% gels) and were transferred to nitrocellulose membrane (Bio-Rad Laboratories, Hercules, CA, USA). Membranes were blocked with 4% BSA or 3% milk-TBST (Tris-buffered saline and 0.05% Tween 20), incubated with the indicated primary antibodies overnight at 4 °C, and then incubated with HRP-linked secondary antibodies at RT for 1 h, washed extensively in TBST, and developed using an

AI600 System (GE Healthcare). To improve the separation of p130Cas by SDS/PAGE, a ratio of acrylamide/bisacrylamide 30 : 0.2 was used.

Immunoprecipitations (see kinase assays, below), pull-downs, and far-western experiments were carried out similarly as in Gemperle *et al.* (2017) and Janošiak *et al.* (2014). For far-western-blot analysis, the protein blots were incubated with 2 $\mu\text{g}\cdot\text{mL}^{-1}$ recombinant human GST-p130Cas (Abcam) or purified mouse GST-p130Cas SH3 diluted in 1% BSA in TBST overnight followed by washing with TBST and incubation (2 h, 4 °C) with anti-GST antibody (Sigma-Aldrich s.r.o.). After extensive washing with TBST, blots were treated with HRP-conjugated secondary antibodies and developed using the AI600 System. Band intensity was determined using FIJI (IMAGEJ; National Institutes of Health; Schindelin *et al.*, 2012).

2.5. Kinase assays

Cells were transfected with either Flag- or StrepII-fused mouse PKN3 (WT or KD) using the PEI transfection reagent (Polysciences) according to manufacturer instructions. After 48 h, cells were washed with PBS and lysed in standard lysis buffer [50 mM Tris/HCl (pH 7.1), 150 mM NaCl, 1% Triton X-100] with protease and phosphatase inhibitors (SERVA Electrophoresis GmbH) and 10 mM glycerol-2-phosphate (Sigma-Aldrich s.r.o.). Proteins were immunoprecipitated with anti-Flag M2 affinity resin (Sigma-Aldrich s.r.o.) and eluted with Flag peptide as described previously (Unsal-Kacmaz *et al.*, 2012). StrepII-fused PKN3 was precipitated with Strep-Tactin[®] Superflow[®] resin and eluted with 1 \times Buffer E (Strep-Tactin Elution Buffer; IBA Lifesciences). Kinase assays were carried out in conditions described previously (Leenders *et al.*, 2004; Unsal-Kacmaz *et al.*, 2012). GFP-fused p130Cas variants (WT, 15AN, S432A; see Plasmid construction section, above) were immunoprecipitated from transiently transfected cells using anti-GFP 3E6 antibody (Thermo Fisher Scientific) and nProtein A Sepharose 4 Fast Flow (GE Healthcare). Subsequently, immobilized p130Cas was dephosphorylated using Lambda protein phosphatase (New England Biolabs) as specified by the manufacturer. Phosphatase was inactivated by two washes with TBS containing 10 mM sodium orthovanadate and 20 mM EDTA, and two washes with TBS and p130Cas variants were eluted with 0.1 M glycine pH 3.5 for 10 min in RT. After elution, pH was equilibrated by adding the corresponding volume of 1 M Tris pH 9.2 and proteins were used as a substrate in reaction with 1 mM ATP γ S (Sigma-Aldrich s.r.o.). After 45 min in 35 °C, reactions were

stopped with EDTA to a final concentration of 20 mM and alkylated with 50 mM *p*-nitrobenzyl mesylate (Abcam) at RT for 2 h. Samples were resolved using SDS/PAGE and immunoblotted using antithiophosphate ester antibody (clone 51-8; Abcam). GSK3-derived peptide fused to GST was prepared and used as a positive control for PKN3 activity as described previously (Unsal-Kacmaz *et al.*, 2012) and its phosphorylation detected by anti-Phospho-GSK-3 α/β antibody. For autoradiography, kinase reactions were performed similarly, with 5 μ Ci [γ -³²P] ATP added to the reaction. The samples were heated for 10 min at 95 °C, resolved using SDS/PAGE, and subjected to autoradiography.

2.6. 2D and 3D migration assays

Scratch-based migration assays in 2D were carried out using an IncuCyte automated imaging system (Essen BioScience, Ann Arbor, MI, USA). Briefly, MEFs with Dox-inducible PKN3 WT were seeded onto 96-well plates (Corning) at a density of 100 000 cells/well (10% serum in DMEM) and half of the wells were supplemented with Dox (final 250 ng·mL⁻¹). After 24 h, monolayers of cells were scratched using a scratching apparatus that produced strongly identical scratches in each well. The IncuCyte system was programmed to obtain real-time phase-contrast images of the wounds every 2 h for 2 days. Cell migration was automatically quantified and expressed as relative wound density, which indicates the ratio of sharpness of the wounded area and of the adjacent nonwounded area. The IncuCyte imaging system was then used to automatically calculate the area of each wound at each time point up to the point of complete closure of the wound from an average of the quadruplicate.

3D cell-zone exclusion assays were carried out using the JuLI™ Br (NanoEnTek, Seoul, Korea) system with two microscopes situated in the incubator. Collagen R solution (4 mg·mL⁻¹; SERVA Electrophoresis GmbH) was diluted to the final mix: 1 mg·mL⁻¹ collagen, 1% serum (to decrease the effect of proliferation), 1× DMEM, 15 mM HEPES (750 mM), 8.5 mM NaOH (1 M), 0.4% NaHCO₃ (7.5%; Sigma-Aldrich s.r.o.), and 5 μ g·mL⁻¹ folic acid. Next, 40 μ L of the collagen mix was then added into each well (total 6) of two 96-well plates and let to polymerize at 37 °C. Cell suspension (100 μ L; 1 × 10⁶ cells·mL⁻¹) noninduced or 24-h Dox-pre-induced cells were added on top of the collagen gel. After cell attachment (4 h), the medium was removed and scratch was performed. Immediately after removal of the rest of media in the generated wound, another layer of collagen mix (100 μ L) was added

(schema of the experiment is shown in Van Troys *et al.*, 2018). Collagen was allowed to polymerize for 15 min at RT to prevent formation of bubbles in the collagen interface, then for another 15 min at 37 °C. Finally, 100 μ L of DMEM with 1% serum supplemented with or without Dox (500 ng·mL⁻¹) was added on the top of each well and CELLTRACKER software (Piccinini *et al.*, 2015) was used to manually track at least 60 random (fastest) (top) migrating cells across the cell/collagen interface in the main focal plane from three independent replicates. To create cell migration/tracking maps, the 'CHEMOTAXIS AND MIGRATION TOOL' version 2.0 (Ibidi GmbH, Martinsried, Germany) was used.

2.7. 2D proliferation and 3D cultures in Matrigel

To determine the difference in cell proliferation capacity among individual clones, an AlamarBlue assay was used. For this, 10 000 cells per well were seeded in a 96-well plate, and after cell attachment (4 h), medium was removed and replaced by a culture medium solution containing 10% AlamarBlue. The plates were further incubated for 2 h at 37 °C prior to initial cell mass measurement followed by replacing with standard medium (\pm Dox if required). Cell growth was then measured again after 72 h using a culture medium solution containing 10% AlamarBlue to assess the increment of cell mass. Absorbance was measured at 570 nm (with reference at 600 nm) using an Infinite M200 PRO microplate reader. As a control, AlamarBlue was added to the cell growth medium without cells. The assay was performed in triplicates and was repeated three times.

xCELLigence RTCA technology, which provides highly standardized experimental conditions and allows for uninterrupted, label free, and real-time analysis of the cells over the course of the experiment, was used to study cell proliferation. The cells were counted (100 000 mL⁻¹) and then separated to supplement one part with Dox (final 250 ng·mL⁻¹) and one part without. Subsequently, 7500–10 000 cells (15 000 cells prior to siRNA transfection) with or without Dox were seeded per well of an xCELLigence E-plate in triplicate, left to sit for 30 min at RT, and then transferred to the xCELLigence RTCA device. Data were collected every 30 (15) min for 48–72 h. Cells were seeded into the wells of the E-plate 24 h prior to siRNA transfection and/or inhibitor treatment. All data were recorded using RTCA Software version 2.0 (ACEA Biosciences, Inc., San Diego, CA, USA), which generated curve-slope values reflecting the speed of cell growth. Cell growth was calculated from the log

growth phase of the curve starting 4- to 9-h post-Dox induction followed by processing in MS Excel and comparison to noninduced controls. E-plates were recycled to remove cells and used repeatedly up to three times.

SC (MDA-MB-231) cells were embedded into Matrigel (Corning) as previously published (Unsal-Kacmaz *et al.*, 2012). In brief, cells grown in 6-cm dishes with or without Dox (siRNA transfected) for 24 h were detached from culture dishes and suspended in Matrigel solution [per well: 80 (50) μL of Matrigel and 20 (10) μL of medium with 10% serum and 20 000 (10 000) cells] at 4 °C. Then, 100 (50) μL of this Matrigel-embedded cell suspension was overlaid on 40 μL of Matrigel in a 96-well plate. The plate was allowed to solidify at 37 °C in the incubator. After 30 min, DMEM \pm Dox [500 (250) $\text{ng}\cdot\text{mL}^{-1}$] was added and replaced every 2–3 days. After 7 days, multicellular clusters were imaged using differential interference contrast microscopy (Nikon-Eclipse TE2000-S; Nikon, Minato, Japan) and analyzed from duplicated wells. Quantification was based on at least three independent experiments.

2.8. Microscopy and immunostaining

Confocal images/movies were acquired using a Leica TCS SP2 or SP8 confocal microscope system equipped with a Leica 63 \times /1.45 oil objective (two HyD detectors and two standard PMT detectors, LEICA LAS-AF software; Leica, Wetzlar, Germany) followed by processing in FIJI.

Cells were seeded on cover slips coated with human FN 10 $\mu\text{g}\cdot\text{mL}^{-1}$ (Thermo Fisher Scientific), grown for 24–48 h, and subsequently fixed in 4% PFA, permeabilized in 0.5% Triton X-100, washed extensively with PBS, and blocked in 3% BSA. The cells were then sequentially incubated with primary antibody (dilution according to manufacturer protocol) for 2 h, secondary antibody for 60 min, and Alexa Fluor 594 phalloidin (Thermo Fisher Scientific) for 15 min, with extensive washing between each step. In addition, slides were mounted with Mowiol 4–88 (475904; Merck Millipore, Burlington, MA, USA) containing 2.5% 1,4-diazobicyclo-[2.2.2]-octane (D27802; Sigma-Aldrich) in the presence or absence of DAPI for nuclear staining and imaged at RT.

Colocalization analyses of PKN3 with p130Cas and actin in lamellipodia were conducted on live cells cotransfected by mCherry-PKN3 variants (mPR, WT, –), GFP-p130Cas, and CFP-fused LifeAct. Alternatively, GFP-PKN3 variants and mCherry-LifeAct were used. The cells were placed on glass-bottom

dishes (MatTek, Ashland, MA, USA) coated with 10 $\mu\text{g}\cdot\text{mL}^{-1}$ FN, transfected, and cultured for 24 h before the experiment. Movies were acquired of cells in DMEM without phenol red supplemented with 10% Serum at 37 °C and 5% CO₂ using a Leica TCS SP2 or SP8 confocal microscope (63 \times /1.45 oil objective). Quantification of mCherry-PKN3 WT, mCherry-PKN3 mPR, and mCherry localization to lamellipodia (lifeActin as marker) was calculated by measuring the signal ratio of mCherry fluorescence in lamellipodium versus in cytosol (5 μm from lamellipodium). A total of 160 measurements (50 living cells) gathered in three independent experiments were performed using FIJI.

Gelatin degradation assay was performed according to the manufacturer instructions (QCM™ Gelatin Invadopodia Assay, Merck Millipore). Cells were seeded on gelatin supplemented with DMEM, 10% serum with or without Dox, and gelatin degradation was assessed after 48 h using a Nikon-Eclipse TE2000-S (10 \times /0.25 or 20 \times /0.40 Nikon objective) followed by processing in FIJI.

Lung metastases on the lung parenchyma were visualized using a Carl Zeiss AxioZoom.V16 fluorescence microscope (Carl Zeiss AG, Oberkochen, Germany) followed by processing in FIJI.

2.9. Subcutaneous mouse tumor models

Nu/nu mice (total 48, $n = 12$ per group), 8-week old, were subcutaneously injected with 1×10^6 GFP-positive SC cells (200 μL of suspension in PBS) that either expressed endogenous PKN3 (group 1) or lacked PKN3 expression (group 2, 3, and 4). These cells expressed mCherry vector (groups 1 and 2), mCherry-fused Flag-PKN3 WT (group 3), or mCherry-fused Flag-PKN3 mPR (group 4) induced by doxycycline hydrochloride, which was administered via Dox pellets (200 $\text{mg}\cdot\text{kg}^{-1}$) on the day of cell injection. After 16 (group 1, faster tumor growth) or 21–22 days (within groups 2–4), tumors were surgically removed under total body anesthesia and their weight was determined, followed by disruption by a tissue tearor in RIPA lysis buffer containing protease inhibitors (SERVA Electrophoresis GmbH) and preclearance by centrifugation at 16 000 g at 4 °C for 30 min. Tissue lysates were normalized to GFP level (Infinite M200 PRO) and analyzed by immunoblotting (SDS/PAGE separation or dot blot) as described in Janoštiak *et al.* (2014). Postoperation, doxycycline hydrochloride was administered via drinking water at 0.2 $\text{mg}\cdot\text{mL}^{-1}$ and supplemented with 1% sucrose. Animals in group 1 were killed 14 days postsurgery, and in groups 2–4 at

21 days postsurgery, and their lungs were collected. Immediately at sacrifice, the right lungs were washed in PBS and viewed under a fluorescence microscope to analyze GFP and mCherry-positive metastases grown on the surface, as well as within the lung parenchyma. Right lungs were fixed for 72 h in 4% PFA for immunohistochemistry analysis. All experiments (surgery, cell transplantation, measurement of tumor weight) were performed blinded and independently by two researchers, and in compliance with the guidelines of the Ministry of Education, Youth and Sports of CR (institutional approval no. 70030/2013-MZE-17214).

2.10. *In silico* analysis

Data of invasive breast carcinoma (1100 tumors in TCGA, provisional) and prostate adenocarcinoma studies (499 tumors, TCGA, provisional) were retrieved from and analyzed using the cBio Cancer Genomics Portal (cbioportal.org; Gao *et al.*, 2013) or processed using the SIGMAPLOT software package (Systat Software, Inc., Point Richmond, CA, USA). The available data on protein phosphorylation levels of p130Cas (BCAR1) were renumbered from isoform 6 (Ser474) to isoform 1 (corresponding to Ser432).

2.11. Statistical analysis

Statistical analyses were performed using the SIGMAPLOT software package (Systat Software, Inc.). Data with a normal distribution were subjected to one-way ANOVA, whereas data failing the normality test were analyzed by one-way ANOVA on ranks followed by Dunn's *post hoc* comparison. All compared groups passed an equal variance test. Where not indicated differently, the same cells treated or not treated by Dox were compared. Graphs were created using GRAPHPAD PRISM 6 (GraphPad Software Inc., La Jolla, CA, USA). Data are reported as the means \pm SD unless otherwise indicated. Correlation statistics were calculated according to the Spearman's rank and Pearson correlation methods. A *P* value of 0.05 was considered as the threshold for statistical significance. *P* values are indicated in the figure legends.

3. Results

3.1. p130Cas directly interacts with PKN3

To confirm the predicted PKN3–p130Cas interaction, we first analyzed the potential of p130Cas SH3 domain variants to pull-down PKN3. The scheme of p130Cas

and PKN3 mutagenesis is shown in Fig. 1A. As predicted, only the p130Cas SH3 WT, but not phosphomimicking mutant variant (Y12E), showed strong association with PKN3 WT. Correspondingly, p130Cas SH3 WT was not able to effectively pull-down a PKN3 variant in which the target polyproline motif was mutated to P₅₀₀APSAPRL (PKN3 mPR; Fig. 1B; 10–50 \times decrease compared to WT; *P* = 0.003). Notably, a kinase-inactivating mutation in the catalytic domain of mouse PKN3 (KD; K577E; Fig. 1A and Fig. S1A) also caused significant decrease (4–20 \times ; *P* = 0.007) of PKN3–p130Cas SH3 interaction (Fig. 1B). Subsequently, we confirmed p130Cas–PKN3 interaction using co-immunoprecipitation analysis. We demonstrated that PKN3 co-precipitates with immunoprecipitated GFP-p130Cas WT and the nonphosphorylatable mutant (Y12F) (Fig. 1C), but not with the phosphomimicking mutant (Y12E), and that p130Cas co-precipitates strongly with immunoprecipitated PKN3 WT, less with PKN3 KD, and almost not at all with PKN3 mPR (Fig. 1D). Finally, using far-western experiments, we confirmed that the p130Cas–PKN3 interaction is direct (Fig. 1E,F).

3.2. PKN3 colocalizes with p130Cas in lamellipodia and podosome rosettes

To further assess the p130Cas–PKN3 interaction, we analyzed the colocalization of p130Cas and PKN3 in cells. Specifically, we analyzed the dynamic localization of p130Cas and PKN3 in p130Cas^{-/-} MEFs co-expressing GFP-p130Cas, variants of mCherry-PKN3, and CFP-LifeAct. We found that both p130Cas and PKN3 were enriched in lamellipodia of MEFs (Fig. 2A; Movies S1 and S2). Localization of the PKN3-mPR mutant to lamellipodia was slightly but significantly impaired (Fig. 2A,B), suggesting that the polyproline sequence of PKN3 is important for its targeting to lamellipodia. However, cells expressing GFP-Flag-PKN3 KD exhibited more pronounced filopodia-like protrusions and the presence of lamellipodia was extremely rare compared to that in cells expressing other variants of PKN3, preventing quantification of PKN3 membrane localization (Fig. S1B and Movie S3).

PKN3 has been recently shown to localize to specific actin-rich structures termed podosome rings and belts in osteoclasts (Uehara *et al.*, 2017). Formation of similar structures, termed podosome rosettes, can be induced in MEFs when transformed by activated Src (SrcF) (Tarone *et al.*, 1985). Notably, p130Cas was shown to be critical for their formation (Brábek *et al.*, 2004). To investigate whether PKN3 localizes

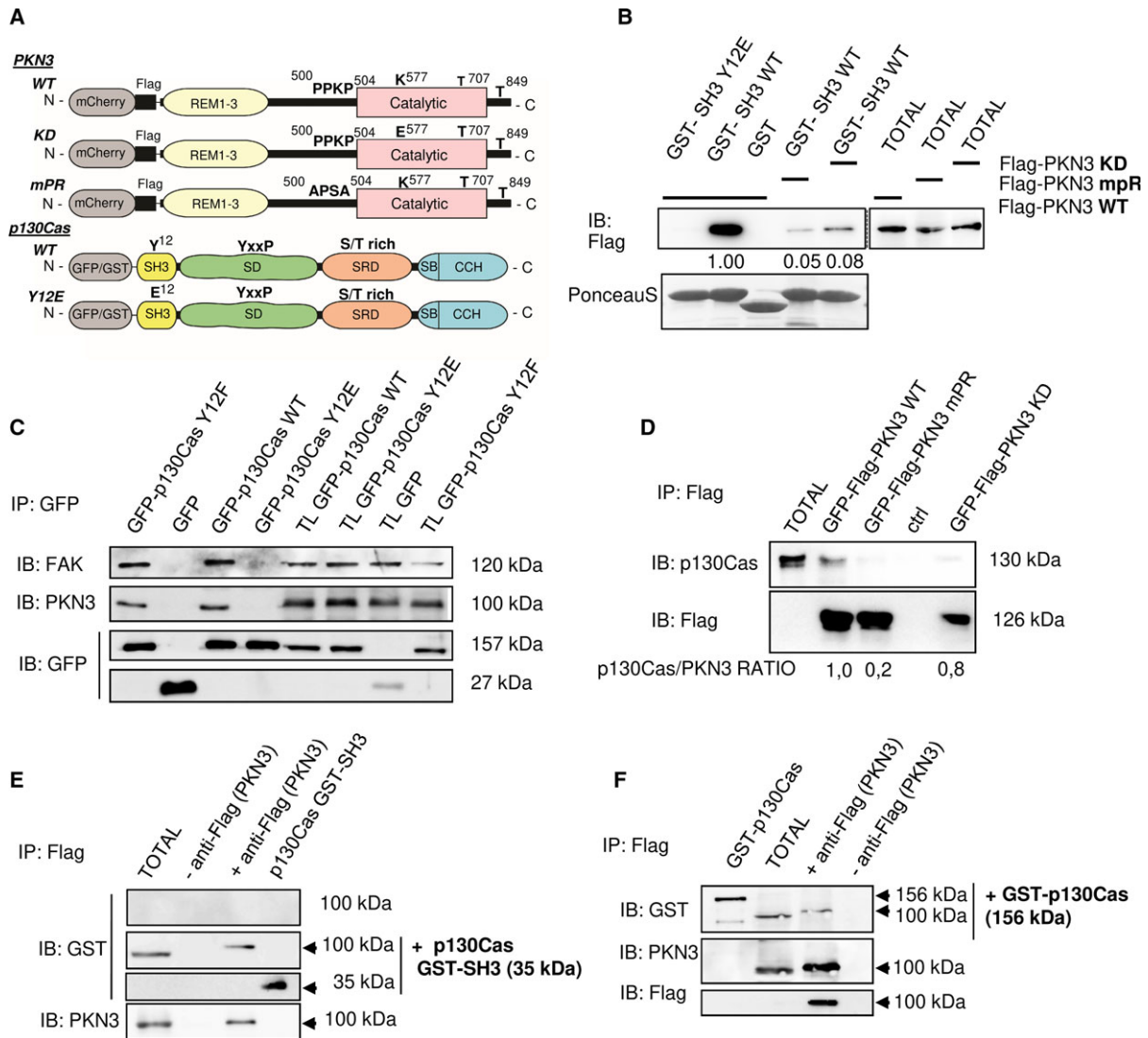


Fig. 1. p130Cas directly interacts with PKN3 (A) Schematic representation of PKN3 and p130Cas domains, important residues, and their mutagenesis. (B) Purified GST-fused p130Cas SH3 variants (WT, Y12E) were used to pull-down Flag-PKN3 variants (WT, mPR, KD), expressed in MEFs. Pulled-down proteins were immunoblotted with anti-Flag antibody and the level of bound PKN3 is indicated relative to Flag-PKN3 WT. GST-SH3 domains were stained with Ponceau-S. GST with lysate from Flag-PKN3 WT was used as a negative control. (C, D) Binding of PKN3 to full-length p130Cas was verified by co-immunoprecipitations. (C) The MDA-MB-231 cells were transiently transfected with indicated mouse GFP-p130Cas variants or GFP alone followed by immunoprecipitations using anti-GFP antibody. Co-immunoprecipitated PKN3 and FAK (as a positive control) were detected using anti-PKN3 antibody or anti-FAK, respectively. (D) The MDA-MB-231 cells were transiently transfected with mouse Flag and GFP-fused PKN3 variants (WT, mPR, KD) followed by immunoprecipitations using anti-Flag sepharose and co-immunoprecipitated p130Cas was detected by anti-p130Cas antibody. Numbers indicate the fold-change in ratio of p130Cas co-immunoprecipitated with PKN3 (relative to PKN3 WT). In far-western experiments (E, F), Flag-PKN3 was immunoprecipitated from transfected MDA-MB-231 cells, transferred to nitrocellulose membrane, and incubated with (E) recombinant GST-p130Cas SH3 domain or (F) whole GST-p130Cas followed by detection with anti-GST antibody. The membrane was then stripped, and both endogenous (endo PKN3) and exogenous PKN3 (exo Flag-PKN3) were detected by anti-PKN3 and anti-Flag antibody, respectively. The upper membrane in E was not incubated with recombinant GST-p130Cas SH3 domain and represents a negative control for anti-GST antibody. As a positive control for GST cross-reactivity, a purified GST-p130Cas SH3 in (E) or whole GST-p130Cas in (F) was ran alongside. TL or TOTAL, total cell lysate; IP, immunoprecipitation; Ctrl, control samples prepared from un-transfected MDA-MB-231 cells.

to podosome rosettes, we expressed the Flag-PKN3 variants in SrcF-transformed p130Cas^{-/-} MEFs re-expressing p130Cas (SC cells) and analyzed their

localization using confocal microscopy on fixed cells. Both PKN3 WT and mPR were enriched in podosome rosettes and colocalized there along with

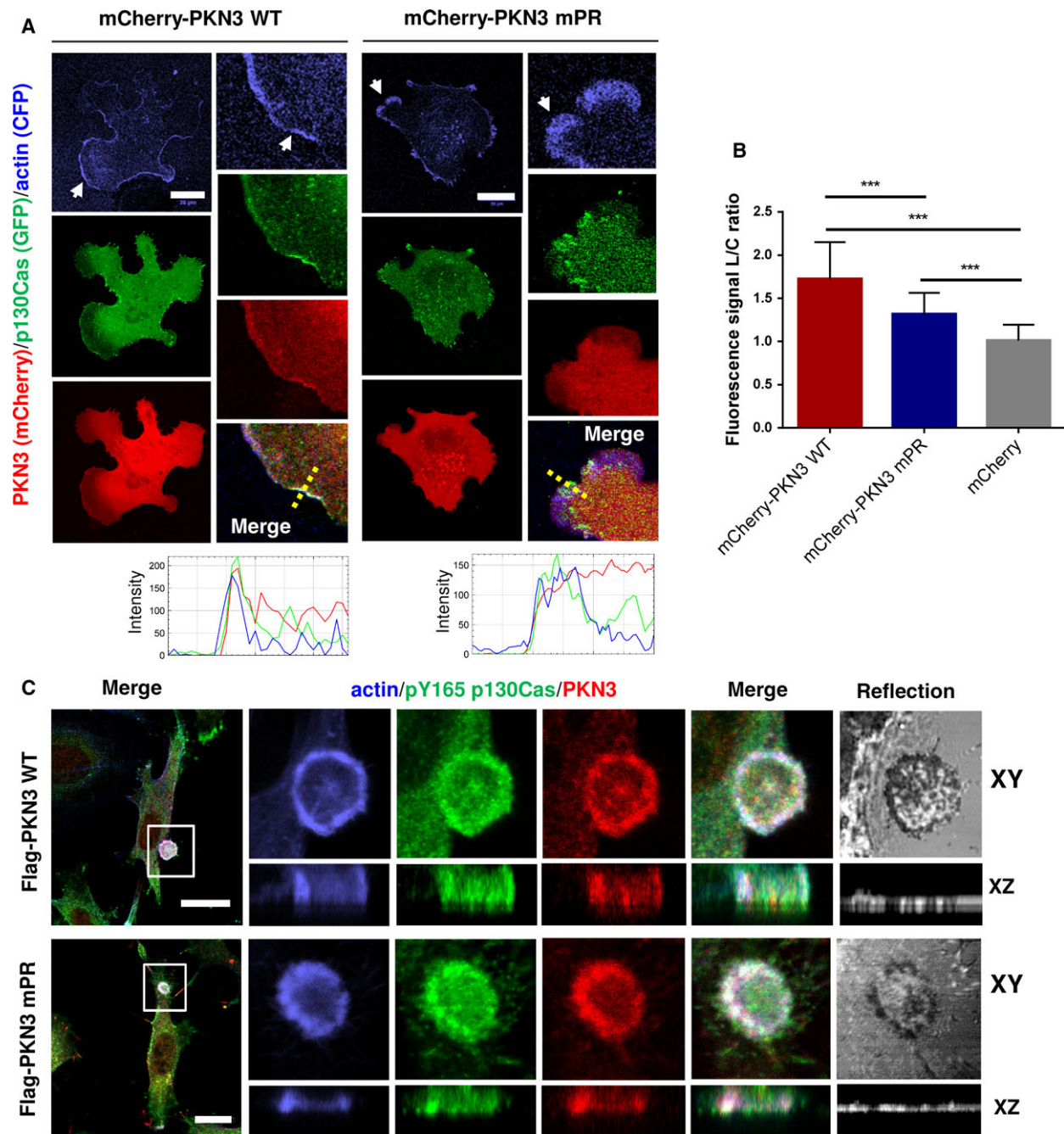


Fig. 2. PKN3 colocalizes with p130Cas in lamellipodia and podosome rosettes. Representative images are shown. (A) p130Cas^{-/-} MEFs plated on fibronectin (FN) were transfected by GFP-p130Cas, CFP-LifeAct, and mCherry-PKN3WT or mCherry-PKN3 mPR and imaged live 24 h after transfection. White arrow indicates lamellipodia. Histogram of dotted straight line is shown. (B) Quantification of mCherry-PKN3 WT, mCherry-PKN3 mPR, and mCherry localization to lamellipodia (LifeAct as marker) was calculated as described in methods (values are mean \pm SD from three independent experiments, $n > 50$ measurements – 3 per cell; *** $P < 0.001$, one-way ANOVA on ranks followed by Dunn’s *post hoc* test). (C) Src-transformed p130Cas^{-/-} MEFs co-expressing p130Cas (SC) and mouse Flag tagged PKN3 WT or Flag-PKN3 mPR are shown. Cells were grown on FN-coated coverslips for 48 h, fixed, and stained for p130Cas by anti-pTyr165 p130Cas antibody (pY165 p130Cas; 2nd 405), for actin by Phalloidin 488 and for Flag-PKN3 by anti-Flag antibody (2nd 633). Reflection (670 nm) indicates fibronectin degradation. All scale bars represent 20 μ m. Cell were imaged by Leica TCS SP8 microscope system equipped with Leica 63 \times /1.45 oil objective.

p130Cas and actin, suggesting that p130Cas is not responsible for PKN3 targeting to podosome rosettes (Fig. 2C).

3.3. PKN3 activity is important for stress fiber formation

In live cell imaging/microscopy experiments, we noticed temporary colocalization of GFP-PKN3 WT or mPR with stress fibers (mCherry-LifeAct) (Fig. S1B,C). As PKN3 downregulation in HUVEC

cells leads to disruption of stress fiber formation (Möpert *et al.*, 2012) and p130Cas expression has been previously shown to affect stress fiber morphology (Honda *et al.*, 1998), we analyzed the importance of PKN3 activity and interaction with p130Cas on stress fiber formation. Therefore, we co-transfected p130Cas-GFP WT and mCherry-Flag-fused PKN3 variants (WT, mPR, KD) or mCherry to p130Cas^{-/-} MEFs (Fig. 3A). Cells expressing PKN3 WT or mPR displayed prominent stress fibers, suggesting that interaction between p130Cas and PKN3 is not important for

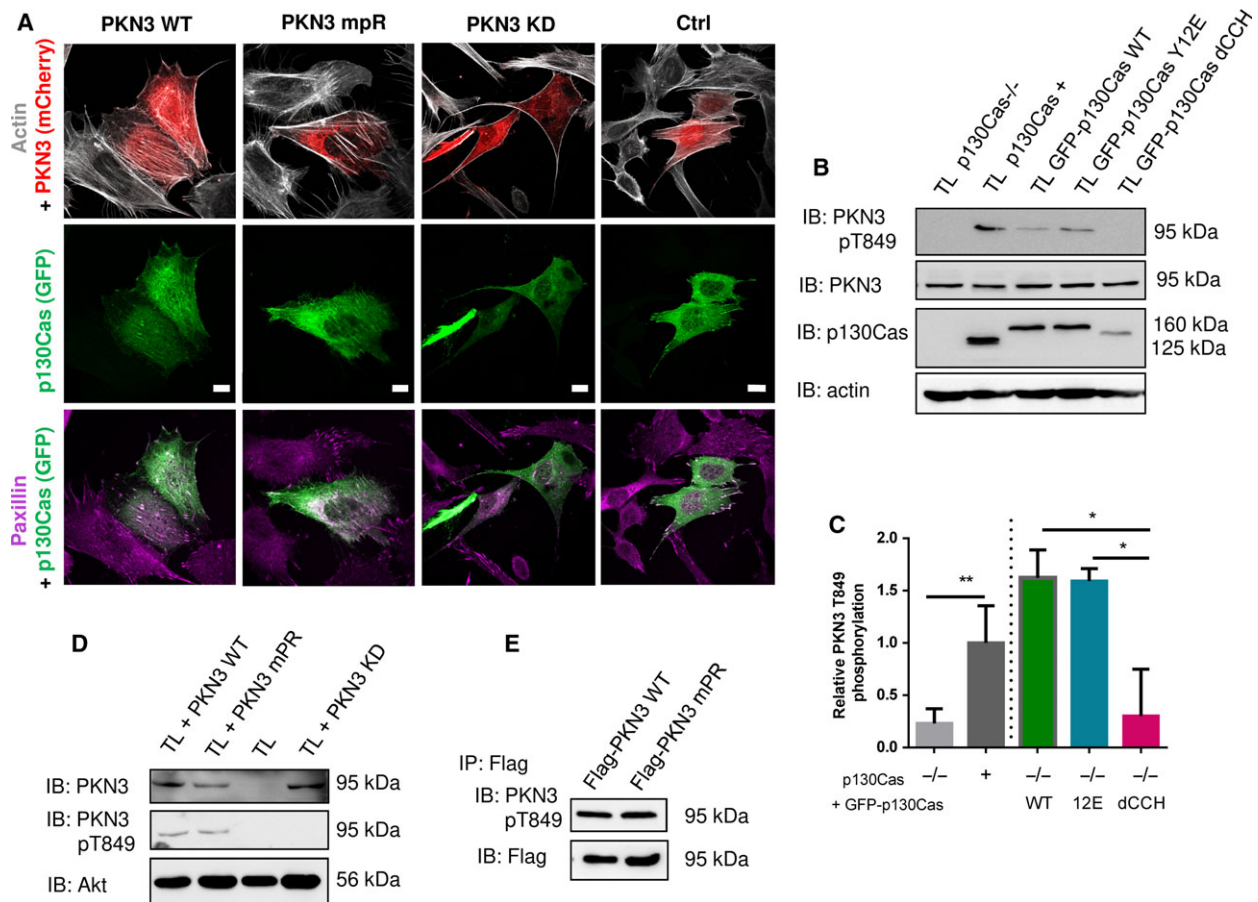


Fig. 3. PKN3 activity is important for stress fibers formation and is stimulated by the expression of p130Cas. (A) p130Cas^{-/-} MEFs growing on FN-coated cover slips were co-transfected by GFP-p130Cas and mCherry-PKN3 fusion variant (WT, mPR, KD) or mCherry. After 48 h, cells were fixed and imaged by Leica TCS SP2 microscope (63×/1.45 oil objective). Stress fibers were visualized by Phalloidin (405) and focal adhesions by anti-Paxillin staining (2nd 633). Representative images are shown. Scale bars represent 20 μm. (B) p130Cas^{-/-} MEFs or p130Cas^{-/-} MEFs re-expressing p130Cas or transfected by GFP-fused p130Cas variants (WT, YE, dCCH) were lysed in RIPA buffer, blotted to nitrocellulose membrane, and analyzed for endogenous PKN3 activity by antibody anti-phosphoThr849 of PKN3 (pT849 PKN3). Expression of p130Cas mutants was verified by anti-p130Cas antibody and loading by anti-PKN3 and anti-actin antibody. (C) Densitometric quantification of PKN3 activity (pT849 PKN3 phosphorylation). The effect of p130Cas re-expression on PKN3 T849 phosphorylation was analyzed separately from the effect of transfected p130Cas mutants (indicated by a dotted line). Error bars indicate means ± SD from three independent experiments (four experiments for the left part). Statistical significance was evaluated by one-way repeated ANOVA followed by Turkey's *post hoc* test (**P* < 0.05; ***P* < 0.01). (D) Lysates or (E) immunoprecipitates (by Flag sepharose) from p130Cas^{-/-} MEFs re-expressing p130Cas and overexpressing PKN3 variants (WT, mPR, KD) were immunoblotted by anti-PKN3, anti-pT849 PKN3, and anti-Akt antibodies (loading control).

stress fiber formation. In contrast, transfection of cells by PKN3 KD greatly reduced stress fiber formation, instead inducing cortical localization of F-actin (Fig. 3A).

3.4. p130Cas stimulates PKN3 kinase phosphorylation on Thr849 independently of p130Cas–PKN3 interaction

It has previously been shown that PKN3 turn motif site phosphorylation (human Thr860, homologous to mouse Thr849) correlates with PKN3 activity and that active PKN3 is predominantly localized in the nucleus (Leenders *et al.*, 2004; Unsal-Kacmaz *et al.*, 2012). To determine whether p130Cas influences PKN3 activation, we analyzed the activity of endogenous mouse PKN3 using an anti-pThr849 antibody in the presence or absence of p130Cas protein. PKN3 phosphorylation on Thr849 was lower in p130Cas^{-/-} MEFs than in p130Cas^{-/-} MEFs re-expressing p130Cas or transfected by GFP-p130Cas (Fig. 3B,C). Expression of the Y12E variant of GFP-p130Cas, which does not bind PKN3, also increased Thr849 phosphorylation of PKN3. Consistent with these findings, the PKN3 mPR mutant, which is unable to bind p130Cas, did not differ with regard to pThr849 phosphorylation status from PKN3 WT (Fig. 3D,E). Notably, however, Thr849 phosphorylation was not increased by expression of GFP-p130Cas without the CCH domain (dCCH) (Fig. 3B,C, and Fig. S1D). PKN3 KD, used as a negative control for anti-pThr849 antibody specificity, was not phosphorylated, as expected (Fig. 3D). Taken together, the data suggest that p130Cas expression induces PKN3 activation and this activation is independent of p130Cas–PKN3 interaction.

3.5. p130Cas–PKN3 co-expression and p130Cas Ser428(432) and PKN3 Thr860 phosphorylation are positively correlated in human breast (prostate) tumors

Previous studies showed positive correlation between PKN3 or p130Cas (BCAR1) protein levels and cancer progression in patients with breast or prostate cancer (Dorssers *et al.*, 2004; Fromont and Cussenot, 2011; Leenders *et al.*, 2004; Nikonova *et al.*, 2014; Oishi *et al.*, 1999; Schultheis *et al.*, 2014; Strumberg *et al.*, 2012). To test the assumed link between PKN3 and p130Cas signaling, we further performed cross-correlation analysis of publicly available transcriptomic data using the cBio Cancer Genomics Portal (cbioportal.org; Gao *et al.*, 2013). We focused on invasive breast carcinoma (1100 tumors in TCGA,

provisional) and prostate adenocarcinoma studies (499 tumors, TCGA, provisional). Within these sets of RNA-Seq data, we evaluated the mRNA expression of PKN3 and p130Cas and ran correlation statistical analysis (Fig. 4A–C). This analysis showed that elevated expression of *PKN3* significantly positively correlates with the elevated expression of p130Cas and vice versa in both patients with breast cancer and those with prostate cancer (Fig. 4A and Fig. S2A). Similarly, the level of p130Cas expression increased with the level of Src kinase, signaling through which is highly associated with p130Cas (Brábek *et al.*, 2004; Fonseca *et al.*, 2004; Fig. 4B and Fig. S2B). In contrast, expression of *PKN2*, which does not possess a p130Cas interaction site and therefore does not suggest crosstalk with the p130Cas signaling circuit, had negative correlation to mRNA levels of p130Cas (Fig. 4C and Fig. S2C,D).

In parallel, we analyzed the available data on protein phosphorylation levels of PKN3 and p130Cas [Clinical Proteomic Tumor Analysis Consortium (CPTAC), MS analysis of 34 invasive breast carcinoma tumors]. Statistical analysis revealed that phosphorylation of PKN3 at Thr860 (homologous to mouse Thr849), which reflects PKN3 activity, and p130Cas at Ser428 (conserved homolog to mouse Ser432 and shown in cBioportal analysis as p130Cas Ser474) exhibits strong positive correlation (Pearson test 0.42, *P* value 0.0134; Spearman test 0.434, *P* value 0.0106; Fig. 4D). Taken together, the cross-correlation analysis of the transcriptomic and phosphoproteomic data showed a positive correlation between PKN3 and p130Cas expression in invasive breast carcinoma and prostate adenocarcinoma tumors, and positive correlation between PKN3 activity and the level of p130Cas phosphorylation on Ser428 in invasive breast carcinoma tumors.

3.6. PKN3 phosphorylates mouse p130Cas on Ser432 *in vitro*

p130Cas has also been previously reported to undergo serine phosphorylation under various conditions, for example, during mitosis or cell adhesion. However, the kinase responsible for the phosphorylation has not yet been identified (Garcia-Guzman *et al.*, 1999; Makkinje *et al.*, 2009; Yamakita *et al.*, 1999). Our cross-correlation analysis of the transcriptomic and phosphoproteomic data showed that phosphorylation of human p130Cas (BCAR1) on Ser428 correlates with increased PKN3 activity, indicating that PKN3 might be responsible for this phosphorylation. Human Ser428 of p130Cas corresponds to

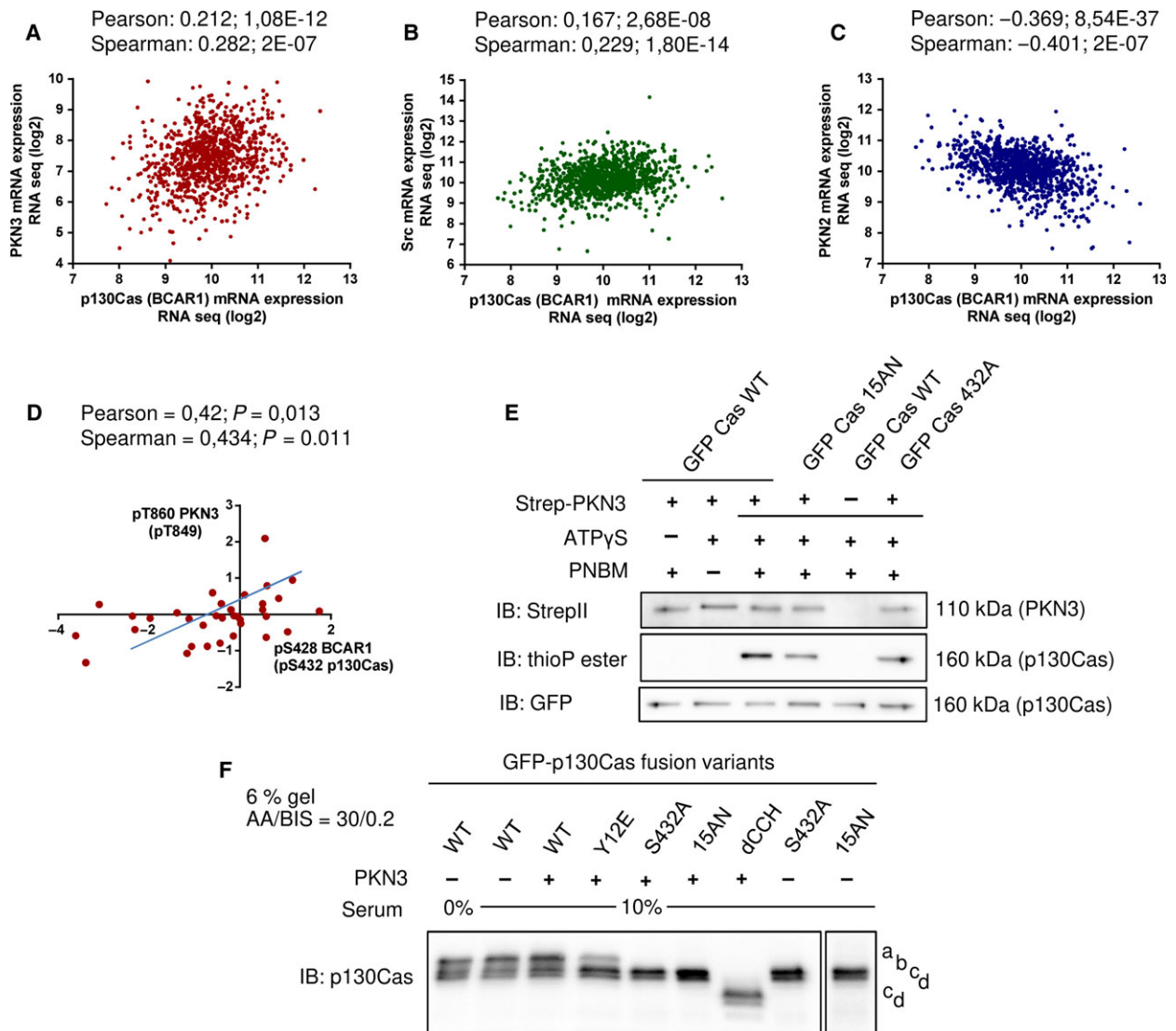


Fig. 4. PKN3 phosphorylates p130Cas and PKN3 activity correlates with p130Cas phosphorylation in human breast carcinomas. (A–C) Correlation statistics (graphs) of publicly available RNA-seq data of co-expression of (A) human p130Cas/BCAR1 and PKN3; (B) p130Cas/BCAR1 and Src; (C) p130Cas/BCAR1 and PKN2 or graph (D) showing positive linear dependency of protein phosphorylation levels (log ratio values) of PKN3 Thr860 and p130Cas/BCAR1 Ser428 in invasive human breast tumors. (E) Kinase reactions *in vitro* with precipitated Strep-PKN3 and GFP fusion p130Cas variants (shown as Cas). Reactions were carried out in the presence of ATP γ S followed by alkylation with PNBM and detection with specific antithiophosphate esters (thioP ester) antibody. Combinations of PNBM (alkylation reagent) or ATP γ S were facilitated to exclude false-positive signals. Antibodies anti-StrepII and GFP were used to detect PKN3 kinase or GFP-fused p130Cas variants, respectively. Representative blots are shown. (F) Lysates from p130Cas^{-/-} MEFs re-expressing GFP-fused p130Cas variants with or without mCherry-PKN3 overexpression were run on SDS/PAGE using an acrylamide/bisacrylamide ratio of 30 : 0.2 followed by immunoblotting and detection by anti-p130Cas antibody. a-d refers to different GFP-p130Cas isoforms.

mouse p130Cas Ser432, which has conserved surrounding sequence (KRLSA) and fits well to the known PKN3 phosphorylation motif (Collazos *et al.*, 2011). As for the majority of p130Cas potential Ser/Thr phosphorylation sites, Ser432 is localized in the p130Cas SRD domain. To test the assumed ability of PKN3 to phosphorylate p130Cas, we prepared a

GFP-fused p130Cas mutant for Ser432 (S432A) and p130Cas mutated in SRD in such a manner that all 15 Ser/Thr sites were substituted with Ala or Asn (15AN). The substitution of several Ser/Thr to Asn, instead of more common substitution to Ala, was used with the aim to preserve the helical structure of the SRD. To determine whether PKN3 could

phosphorylate p130Cas in the SRD domain, we performed kinase assays *in vitro* with precipitated Strep-Flag-PKN3 and newly prepared GFP-p130Cas variants (WT, 15AN, and S432A) in the presence of ATP γ S followed by detection with a specific antibody against antithiophosphate ester (Fig. 4E). GFP-p130Cas WT exhibited the highest thiophosphorylation compared to GFP-p130Cas 15AN and Ser432A, which were thiophosphorylated to a similar extent. Partial thiophosphorylation of GFP-p130Cas 15AN indicated that PKN3 could phosphorylate p130Cas also outside SRD domain (Fig. 4E; see Fig. 1A). Notably, PKN3 autophosphorylation was also observed (Fig. S2E). These results verified the presence of a PKN3 phosphorylation motif in the sequence surrounding Ser432 and indicated that PKN3 phosphorylates p130Cas on Ser432 *in vitro*.

Protein p130Cas, similarly to Nedd9 (another member of the p130Cas family; HEF1), exists in cells in two main isoforms, which are attributed to different Ser/Thr phosphorylation (Hivert *et al.*, 2009; Makkinje *et al.*, 2009). Depending on the cell type, p130Cas protein is present upon SDS/PAGE as a single protein or detected as a doublet with the increased proportional representation of the upper band correlating with cell aggressive properties (Janoštiak *et al.*, 2011; Makkinje *et al.*, 2009). To test the biological relevance of p130Cas Ser432 phosphorylation in cells, we prepared lysates from p130Cas^{-/-} MEFs with reintroduced GFP-p130Cas mutants with or without overexpression of mCherry-PKN3 WT and examined the p130Cas migration profile after separation on SDS/PAGE using an acrylamide/bisacrylamide ratio of 30 : 0.2 (Fig. 4F), which improves the separation of Ser/Thr phosphorylation-induced gel shifts, similarly to Hivert *et al.* (2009). GFP-p130Cas WT migrated as four bands with the most pronounced form migrating the slowest. GFP-p130Cas Y12E displayed a shift of the p130Cas protein content from the slowest migrating band toward faster migrating forms. In comparison, the 15 Ser/Thr mutations (15AN) migrated only in the form of two faster bands, similarly to the single mutation of Ser432 (S432A mutant), and were not changed by PKN3 overexpression (Fig. 4F). Furthermore, GFP-p130Cas without the CCH domain also migrated in the form of two faster bands. We concluded that p130Cas SH3 and CCH domains are important for p130Cas Ser/Thr phosphorylation and that the presence of the slowest migration form of p130Cas is associated with Ser432 phosphorylation. However, we failed to promote a switch of the slower migrating p130Cas (WT) isoform to faster ones by serum starvation (Fig. 4F) or by maintaining the cells in suspension

(Fig. S2F); therefore, we could not demonstrate the change of p130Cas WT SDS/PAGE migration pattern by PKN3 overexpression.

3.7. PKN3 overexpression regulates the growth of MEFs in a PKN3-p130Cas interaction-dependent manner

Both PKN3 and p130Cas have been implicated in the regulation of malignant cell growth (Cabodi *et al.*, 2006, 2010b; Leenders *et al.*, 2004). Although PKN3 is scarce in normal human adult tissues except in endothelial cells (HUVECs) (Aleku *et al.*, 2008), a recent study showed that PKN3 is also present in moderate levels in MEFs, supporting these cells as a physiologically relevant model (Mukai *et al.*, 2016). To investigate whether PKN3 regulates cell proliferation in MEFs and whether this is dependent on p130Cas, we prepared stable MEF cells with doxycycline (Dox) inducible mCherry-fused PKN3 WT or mCherry alone in the p130Cas null background with or without re-expression of p130Cas (Fig. 5A). mCherry-PKN3 WT expression started from 5 h and reached saturation within 24 h post-treatment with Dox (Fig. 5B). Cell morphology was unaffected by mCherry-PKN3 WT expression; however, starting 5 h after adding Dox, MEFs re-expressing p130Cas exhibited increased growth rate compared to noninduced controls (Fig. 5C). Induction of mCherry alone as an additional control had no effect and the growth rate of p130Cas^{-/-} MEFs was not affected by PKN3 expression (Fig. 5D,E), indicating that the PKN3-mediated regulation of cell growth was p130Cas-dependent.

To investigate whether PKN3-mediated induction of cell growth rate required PKN3 interaction with p130Cas, we prepared stable cell lines of p130Cas^{-/-} MEFs re-expressing p130Cas with Dox-inducible Flag-fused PKN3 variants (WT, mPR, KD) (Fig. 5F). Only, the induction of expression of PKN3 WT, but not mPR or KD, led to the increase of cell growth compared to that in noninduced controls (Fig. 5G). Increase of cell proliferation induced by PKN3 variants was also verified by AlamarBlue assay (Fig. S3A) with similar outcome.

To test whether PKN3 promoted cell growth of MEFs by phosphorylation of the p130Cas SRD domain, we reintroduced GFP-p130Cas variants (WT, 15AN) or GFP as control to p130Cas^{-/-} MEFs with Dox-inducible mCherry-PKN3 (Fig. S3B). Both GFP-p130Cas WT and 15AN, but not GFP alone, changed cell morphology, as characterized by an increased number of cell protrusions (Fig. S3C). This morphology was not changed by Dox-inducible mCherry-PKN3,

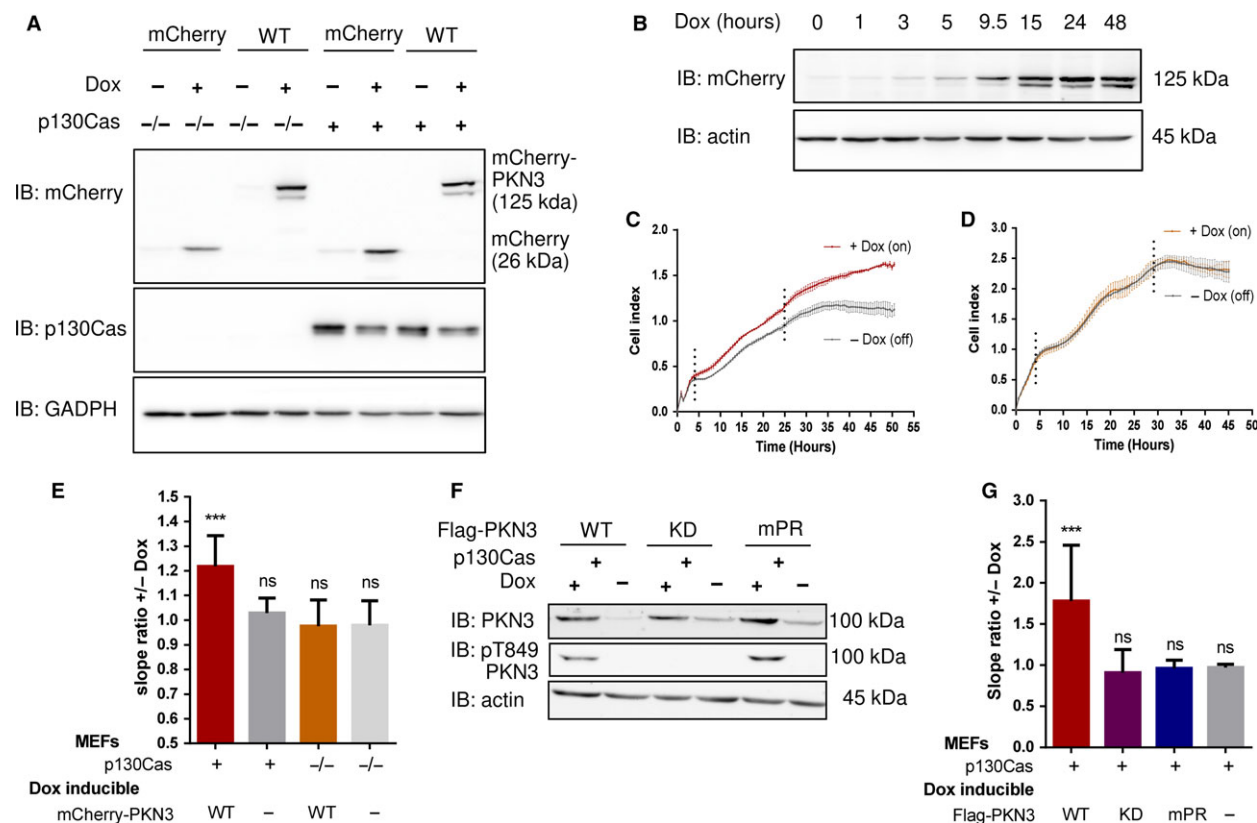


Fig. 5. PKN3 overexpression regulates growth of MEFs, and this effect requires PKN3-p130Cas interaction. (A) Immunoblotted lysates from MEFs p130Cas^{-/-} or MEFs p130Cas^{-/-} re-expressing p130Cas (p130Cas⁺) treated by Doxycycline (Dox) to induce expression of mCherry-PKN3 or mCherry alone. p130Cas presence was detected by anti-p130Cas antibody and mCherry epitope by anti-mCherry antibody. (B) Dynamics of mCherry-PKN3 expression after supplementation with Dox shown by immunoblot with anti-mCherry antibody. (C–E) Effect of induced mCherry-PKN3 expression on cell growth. Representative graphs showing growth of MEFs p130Cas^{-/-} re-expressing p130Cas (p130Cas⁺) (C) or MEFs p130Cas^{-/-} (D) measured in real-time using the xCELLigence RTCA (real-time cell analysis) system instrument. (E) Quantification of cell growth change induced by mCherry-PKN3 expression ('-' indicates inducible mCherry expression used as negative control). Slope ratios reflecting cell growth were calculated from the log growth phase of cell growth (indicated by dotted lines; see C and D). (F) Immunoblotted lysates from MEFs p130Cas^{-/-} re-expressing p130Cas (p130Cas⁺) treated or not treated by Dox which induced expression of Flag-fused PKN3 variants (WT, mPR, KD, empty vector). Stimulated overexpression of PKN3 was detected by anti-PKN3 antibody and its activity by antibody anti-pT849 PKN3. (G) Quantification of cell growth change stimulated by Dox-inducible expression of Flag-fused PKN3 variants (WT, mPR, KD) in MEFs p130Cas^{-/-} re-expressing p130Cas (p130Cas⁺). All error bars indicate means \pm SD calculated from 3 to 5 independent experiments (each in triplicates). Statistical significance was always calculated between induced and noninduced cells and evaluated by one-way repeated ANOVA followed by Turkey *post hoc* test (***) $P < 0.001$.

although Dox treatment increased the growth of cells expressing GFP-p130Cas WT and 15AN compared to that of noninduced controls (Fig. S3D). Therefore, the effect of PKN3 on cell growth was probably independent of p130Cas SRD domain phosphorylation.

To investigate which signaling pathways are involved in the accelerated cell growth induced by PKN3, we analyzed the activation status of p130Cas known downstream/upstream targets ERK, Akt, MLC, mTOR, Src, and STAT3 signaling (Fig. S4A). In agreement with previous PKN3 studies, we did not find any significant changes (Leenders *et al.*, 2004). Only, Src activity was slightly increased by PKN3 expression in a p130Cas-

dependent manner, which is consistent with a recent study demonstrating that PKN3 could promote Src activity in osteoclasts (Fig. S4A,B) (Uehara *et al.*, 2017). Taken together, these results indicated that PKN3 regulates the growth of MEFs and that this effect requires PKN3-p130Cas interaction independently of p130Cas SRD domain phosphorylation.

3.8. Interaction of p130Cas with PKN3 is required for PKN3-dependent increase of invasiveness

The localization of PKN3 in lamellipodia suggests its importance in cell migration. In p130Cas^{-/-} MEFs re-

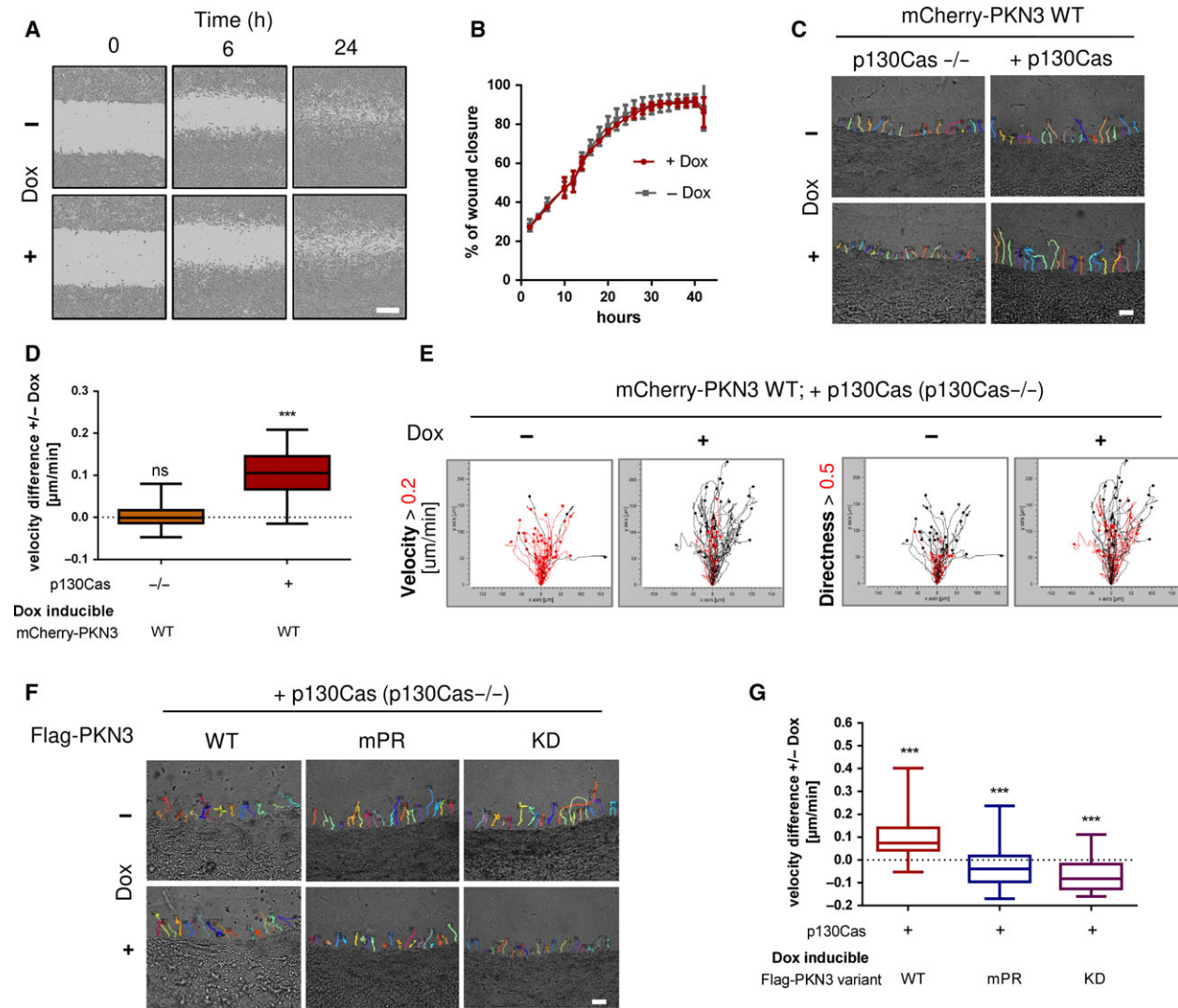


Fig. 6. The interaction of p130Cas with PKN3 is required for PKN3-dependent increase of invasiveness but not 2D migration. (A, B) 2D migration analyzed by wound healing assay. (A) Representative images of MEFs p130Cas^{-/-} re-expressing p130Cas with or without 24 h pre-induced for Flag-PKN3 expression at the time of wounding (0 h), after 6 and 24 h are shown (scale bar 300 μm). (B) Representative graph. (C–G) Cell invasiveness analyzed by 3D cell-zone exclusion assay. Cell migration into collagen was recorded using time-lapse video microscopy with frames being collected every 5 min for 18 h, starting 2 h after collagen scratch, with or without Dox supplementation. Expression of different constructs was pre-induced day before. (C) Representative tracking maps of cells (MEFs p130Cas^{-/-} or MEFs p130Cas^{-/-} re-expressing p130Cas) migrating into collagen supplemented with or without Dox for induction of mCherry-PKN3 expression (scale bar 100 μm). Relevant Movies S4 and S5 are included. (D) Quantification of cell migration velocity difference induced by Dox-inducible mCherry-PKN3 expression in the p130Cas null background with or without re-expression of p130Cas. (E) Migration maps comparing the velocity and directionality of cells described in D). The boxed traces represent the length (above 0.2 μm black, below red) and directionality (above 0.5 black, below red) of cell movement of each individually tracked cell plotted from the same point of origin. (F) Representative tracking maps of MEFs p130Cas^{-/-} re-expressing p130Cas migrating into collagen supplemented with or without Dox for induction of Flag-PKN3 variant expression as indicated (scale bar 100 μm) and their quantification (G). Box and whisker graphs show quantification of cell migration into collagen out of three independent experiments (*n* = 60 cells). Statistical significance comparing induced and noninduced cells was evaluated by one-way ANOVA or one-way ANOVA on ranks followed by Turkey *post hoc* test (***) *P* < 0.001).

expressing p130Cas, we analyzed the effect of inducible expression of PKN3 on 2D migration using a wound healing assay. We found that PKN3 expression has no

effect on the 2D migration on either plastic or fibronectin (FN) (Fig. 6 A and B). These results are consistent with a study of Lachmann *et al.* (2011) where

only siRNA anti-PKN1 or anti-PKN2, but not anti-PKN3, had an effect on wound healing closure of 5637 bladder tumor cells.

Next, we investigated the potential role of PKN3 in invasive cell migration in 3D collagen. To analyze the effect of PKN3 on cell invasiveness, we utilized a 3D cell-zone exclusion assay as characterized in Van Troys *et al.* (2018). In this assay, a monolayer of cells grown on a thick layer of collagen is wounded, and then, the system is overlaid with another layer of collagen. The cells migrating into the wound adopt the morphology and mechanisms of movement of cells migrating in 3D but can be monitored in one focal plane and their movement can be easily tracked and analyzed as in 2D (details described in Materials and methods). p130Cas^{-/-} MEFs re-expressing p130Cas clearly moved faster and more individually compared to p130Cas^{-/-} MEFs (Fig. 6C,D, and Movie S4 versus S5). Induced expression of PKN3 in p130Cas^{-/-} MEFs (Fig. 6C,D, and Movie S5) was not sufficient to increase cell migration or to promote individual cell movement. In contrast, activation of PKN3 expression in p130Cas^{-/-} MEFs re-expressing p130Cas led to an increase of cell speed and invading distance compared to that in noninduced cells but did not change cell directionality (Fig. 6C–E, and Movie S4). Notably, induced expression of PKN3 mPR and KD variants did not induce invasiveness of p130Cas^{-/-} MEFs re-expressing p130Cas (Fig. 6F,G) but rather had the opposite effect, suggesting that PKN3–p130Cas interaction and PKN3 activity are important for PKN3-induced cell invasiveness of MEFs in collagen.

To test whether PKN3 promotes the invasiveness of MEFs by phosphorylation of the p130Cas SRD domain, we performed the 3D cell-zone exclusion assay with p130Cas^{-/-} MEFs re-expressing GFP-p130Cas variants (WT, 15AN) or GFP as control with or without Dox to induce mCherry-PKN3. Re-expression of GFP-p130Cas (WT or 15AN) caused an increase of cell invasive capability in 3D collagen (Fig. S4C). Cell treatment by Dox further slightly increased the migration velocity of cells re-expressing both GFP-p130Cas WT and GFP-p130Cas 15AN in collagen compared to that of noninduced controls (Fig. S4C,D), indicating that phosphorylation of p130Cas in the SRD domain by PKN3 is not involved in the PKN3-dependent increase of MEF invasiveness. Taken together, our results suggest that PKN3 expression increases cell invasiveness of MEFs and that this induced invasiveness is dependent on p130Cas. Furthermore, the PKN3 activity and its ability to interact with p130Cas are required for PKN3-induced cell invasiveness of MEFs,

but is independent of PKN3-mediated phosphorylation of the p130Cas SRD domain.

3.9. PKN3 regulates growth of Src-transformed MEFs and breast cancer cells in p130Cas-dependent manner

Having established the importance of the PKN3–p130Cas interaction for cell proliferation and cell migration in a 3D environment, we next analyzed whether this interaction also influences the growth and invasive behavior of SrcF-transformed cells. We first analyzed the effect of SrcF-induced transformation on the level of endogenous PKN3. We found that PKN3 expression is significantly increased in MEFs transformed by activated Src (almost 2×; $P < 0.009$) and that this increase is dependent on the presence of p130Cas (Fig. 7A and Fig. S7A). To reduce the contribution of endogenous PKN3 in subsequent experiments, we inactivated PKN3 in SrcF p130Cas^{-/-} MEFs re-expressing p130Cas (SC cells) using CRISPR/CAS9 system (Materials and methods; Fig. 7B). All PKN3 KO clones (SCpkn3^{-/-}) tested exhibited significantly reduced proliferation compared to the parental cells (Fig. 7C). Consistent with this, reintroduction of PKN3 (mCherry-Flag-fused), but not PKN3 mPR or mCherry alone, under a Dox-controlled promoter (Fig. 7D) led to rescue of cell growth in SCpkn3^{-/-} cells when Dox was supplemented to the medium (Fig. 7E and Fig. S7B).

To mimic the tumor environment, we further examined the growth of SCpkn3^{-/-} cell lines in a 3D environment, similarly as reported in Unsal-Kacmaz *et al.* (2012). Induced expression of PKN3 in SCpkn3^{-/-} cells promoted a more aggressive behavior characterized by the appearance of a larger number of multicellular clusters in 3D Matrigel when compared to that in uninduced cells (Fig. 7F,G). In contrast, inducible expression of PKN3 mPR did not significantly change cell growth. To further confirm our results that PKN3 supports aggressive cell behavior of SrcF-transformed MEFs in Matrigel, we also established stable SC cell line inducibly expressing shRNA anti-endogenous PKN3 (Fig. 7F–H). Consistent with the previous findings, the enhanced growth of parental SC cells compared to that of SCpkn3^{-/-} cells was reduced by Dox-induced shRNA anti-PKN3 to a basal level of SCpkn3^{-/-} cells (Fig. 7G). Taken together, these results suggested that PKN3 supports a more malignant phenotype in SrcF MEFs and that interaction of PKN3 with p130Cas may at least partly mediate this effect.

To verify the involvement of p130Cas (BCAR1) in PKN3-induced cancer progression, we performed a set

of experiments with MDA-MB-231 breast cancer cells. First, to reduce the contribution of highly expressed endogenous PKN3 (Lachmann *et al.*, 2011) in subsequent experiments, we inactivated *PKN3* gene using CRISPR/CAS9 system (Materials and methods; Fig. 7I) and tested the effect of reintroduced human PKN3 on cell proliferation (Fig. 7J,K). Consistent with our results obtained in SrcF-transformed MEFs, Dox-induced expression of PKN3 fused to mCherry, but not mCherry alone, reproducibly increased cell growth (Fig. 7K and Fig. S5A). To analyze an involvement of p130Cas in this verified PKN3-driven phenotype, we depleted p130Cas in these cells with siRNA (Fig. 7L). Consistent with our results obtained in SrcF-transformed MEFs, the knockdown of p130Cas in MDA-MB-231 *pkn3^{-/-}* cells (MDApkn3^{-/-}) blocked PKN3-promoted increase of cell growth compared to noninduced controls in p130Cas dose-dependent manner (Fig. 7L and Fig. S5B). The level of p130Cas also correlated with cell survival as siRNA transfection was slightly toxic under these conditions (Fig. S5B). We next analyzed the involvement of p130Cas in the previously demonstrated PKN3 ability to support a more aggressive growth of MDA-MB-231 cells in the 3D Matrix (Unsal-Kacmaz *et al.*, 2012). In agreement with work of Unsal-Kacmaz *et al.*, we observed that Dox-induced expression of PKN3 promoted aggressive growth (Fig. 7M,N). This effect was abolished by p130Cas knockdown, indicating that p130Cas is indeed required for PKN3-induced cell growth.

Having verified the influence of p130Cas in PKN3-dependent increase of cell growth in MDA-MB-231 cells, we also investigated the potential role of PKN3 in invasive MDA-MB-231 cell migration in 3D collagen. In contrast to results obtained in MEFs, however, inducible expression of PKN3 did not further increase invasive migration of MDApkn3^{-/-} cells (Fig. S5C,D).

To investigate which signaling pathways are involved in the accelerated cell growth of MDA-MB-231 cells induced by PKN3, we analyzed the activation status of p130Cas known downstream/upstream targets. Similarly to results obtained in MEFs, the average activation status of Src (Src Tyr416), FAK (Tyr397), mTOR signaling (Phospho-S6 Ribosomal Protein), and p130Cas migration pattern on SDS/PAGE were not significantly altered by inducible expression of PKN3 (Fig. S5E and Fig. 7J) or by siRNA-mediated knockdown of endogenous human PKN3 (Fig. S5F). To elucidate at least to some extent the mechanism underlying PKN3-induced increased cell proliferation, we next treated MDApkn3^{-/-} cells with a panel of different inhibitors and analyzed their impact on

PKN3-induced cell growth (Fig. S6A). Notably, inhibitors that targeted signaling pathways known to be directly related to p130Cas (PF 573228 – FAK/PYK2; Saracatinib – Src, Latrunculin – Actin; Rapamycin – mTOR) blocked PKN3-induced cell growth (Fig. S6B, C). In contrast, MAPK signaling (CI-1040 – MEK1/MEK2; BIRB796 – p38), CDK4/CDK6 (Palbociclib), EGFR (Gefitinib), or MLCK (ML-7) kinase were not involved (Fig. S6B,D). Inhibitor SB202190 (primary p38 inhibitor) that has been shown to target effectively PKN3 (0.004 μ M) (Falk *et al.*, 2014) also blocked PKN3-induced cell growth and served as positive control. Taken together, these results suggest that functional complex between PKN3 and p130Cas supports a more advanced malignant phenotype in breast cancer cells.

3.10. Interaction of p130Cas with PKN3 regulates invasiveness of Src-transformed MEFs and is required for PKN3-dependent tumor growth *in vivo*

p130Cas has been previously shown to be crucial for invasion of SrcF-transformed MEFs (Brábek *et al.*, 2004). To investigate whether PKN3 could influence the migration of SrcF-transformed MEFs in a 3D environment, we used the 3D cell-zone exclusion assay. In agreement with the results obtained in untransformed MEFs, in SCpkn3^{-/-} cells, induction of PKN3 but not PKN3 mPR expression led to an increase of cell invasion (Fig. 8A,B). Consistent with this, inducible downregulation of PKN3 in parental SC cells by shRNA led to a decrease of cell migration in collagen (Fig. 8A,B).

p130Cas and Src are critical components of podosome-like structures, which are involved in degradation of the ECM (Brábek *et al.*, 2004). As we had shown that PKN3 is also localized to podosome-like structures, we next tested whether the increased invasiveness of PKN3 overexpressing cells was due to their elevated ECM degradation activity. We analyzed the podosome-associated proteolytic activity by gelatin degradation assay and found that gelatin degradation in SCpkn3^{-/-} cells is not affected by the expression of PKN3 (Fig. 8C). These results indicated that the induced invasiveness of SCpkn3^{-/-} cells expressing PKN3 was reflective of a PKN3-induced migratory phenotype rather than increased degradation of ECM.

Nevertheless, PKN3 was recently demonstrated to be necessary for the bone degradation/resorption activity of osteoclasts, similar to that found for p130Cas (Nagai *et al.*, 2013; Uehara *et al.*, 2017). In both cases, an intact polyproline sequence of PKN3 and the

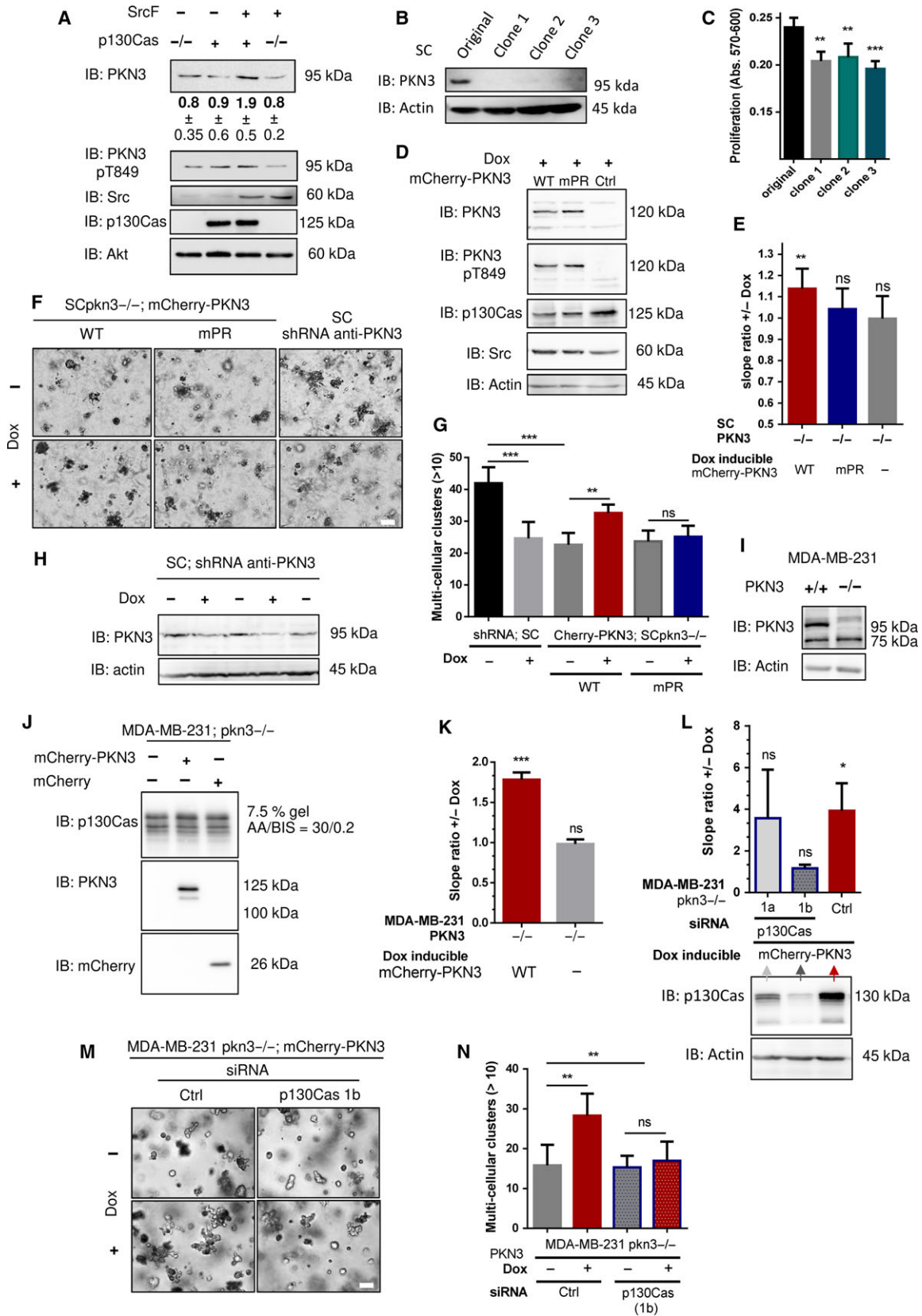


Fig. 7. PKN3 regulates growth in 2D and in 3D environment of Src-transformed MEFs through interaction with p130Cas. (A) Immunoblot of MEFs p130Cas^{-/-} re-expressing p130Cas with or without transformation by constitutively active Src (SrcF, SC cells) and antibodies used as indicated (anti-Akt served as loading control). Densitometric quantification of protein PKN3 amount is indicated below. (B) Immunoblot of SC cells and SC cells with *PKN3* gene inactivated using CRISPR/CAS9 (SCpkn3^{-/-}). Inactivation of PKN3 expression is visualized by antibody anti-PKN3. Antibody anti-actin was used as loading control. (C) Quantification of SC cells proliferation rate with or without inactivated *PKN3* gene cassette by AlamarBlue method (72 h after cell seeding). The graph shows mean absorbance measurement at 570 nm with reference at 600 nm corrected for the initial deviations of cell seeding counts. (D) Immunoblotted lysates from SCpkn3^{-/-} cells treated by Dox to induce expression of mCherry-PKN3, mCherry-PKN3 mPR, or mCherry alone. PKN3 constructs were detected by anti-PKN3 and anti-pT849 PKN3 antibodies, Src and p130Cas by antibodies as indicated. Antibody anti-actin served as loading control. (E) Quantification of cell growth change induced by Dox-inducible mCherry, mCherry-PKN3 WT, or mCherry-PKN3 mPR expression in SCpkn3^{-/-} cells measured by xCELLigence RTCA system. Slope ratios reflecting cell growth were calculated from the log growth phase of cell growth (representative curves are shown in Fig. S7B). (F) SC and SCpkn3^{-/-} cells stably expressing mCherry-PKN3 WT, mPR, or shRNA anti-PKN3 in Dox-dependent manner were embedded into Matrigel. Photographs were taken on day 7, scale bar represents 100 μ m; enlarged image for each sample is shown with subtracted background using IMAGEJ. (G) Multicellular clusters (> 10 cells) indicating proliferating cells were quantified relative to individual cells or small cell aggregates on day 7. Average mean is shown. (H–J) Immunoblots showing (H) effectiveness of PKN3 knockdown in SC cells, (I) MDA-MB-231 cells and MDA-MB-231 cells with *PKN3* gene inactivated using CRISPR/CAS9 (MDApkn3^{-/-}), and (J) engineered MDApkn3^{-/-} cells treated by Dox to induce expression of mCherry-PKN3 or mCherry alone. PKN3 expression is visualized by antibody anti-PKN3. Antibody anti-actin (p130Cas) was used as loading control. (K–N) Effect of induced PKN3 expression on MDApkn3^{-/-} cell growth. (K, L) Quantification of cell growth change induced by Dox-inducible mCherry-PKN3 WT (mCherry alone) measured by xCELLigence RTCA system. Slope ratios reflecting cell growth were calculated from the log growth phase of cell growth (representative curves are shown in Fig. S5A,B). Cells in (L) were transfected by siRNA as indicated in this figure, 6–24 h before medium exchange +/- Dox. The effectiveness of p130Cas knockdown after 48 h is shown by immunoblot using anti-p130Cas antibody. (M) Cells were transfected with siRNA as indicated and 24 h after embedded in 80% Matrigel \pm Dox. Photographs taken on day 7, scale bar represents 100 μ m. (N) Quantification for (M) as described above in (G). Error bars indicate means \pm SD (C, E, G, N), \pm SEM (K, L) calculated from 3 to 5 independent experiments (each in triplicates C, E; in duplicates G, L, N). Statistical significance comparing induced and noninduced cells (E, G, K, L, N) was evaluated by one-way repeated ANOVA followed by Turkey *post hoc* test (* P < 0.05; ** P < 0.01), among variants/groups (C, G, N) by one-way ANOVA followed by Turkey *post hoc* test (** P < 0.01; *** P < 0.001).

p130Cas SH3 domain were required, as we had validated for PKN3–p130Cas binding, and both sequences were implicated in osteoclast function through an association with Src. We thus hypothesized that the Src–PKN3 interaction is indirect and mediated by p130Cas and tested this by co-immunoprecipitation experiments from SrcF-transformed p130Cas^{-/-} MEFs with or without p130Cas re-expression. As predicted, we found that Src failed to co-precipitate with PKN3 in the absence of p130Cas, confirming that the Src–PKN3 interaction is indirect (Fig. 8D). Furthermore, we observed PKN3 binding to actin in a p130Cas-dependent manner (Fig. 8D).

As both PKN3 and p130Cas enhance cell proliferation *in vitro* and can contribute to various stages of tumor development *in vivo* (Leenders *et al.*, 2004; Tornillo *et al.*, 2014; Unsal-Kacmaz *et al.*, 2012) and to expand our results showing *in vitro* functional relevance of the PKN3–p130Cas interaction to *in vivo* analysis, we subcutaneously injected SCpkn3^{-/-} cells stably engineered for inducible expression of either PKN3 WT or PKN3 mPR fused to mCherry, or mCherry alone, into nu/nu mice (total 48). As a positive control, a parental line of SC cells inducibly expressing mCherry was used. The animals were split into four groups (12 per group), all treated with Dox to induce the expression of

mCherry-fused PKN3 variants or mCherry alone. The primary tumors were surgically removed at days 21 and 22 after inoculation for the SCpkn3^{-/-} cell lines (+PKN3 WT, +mCherry, and +PKN3 mPR, respectively) and at day 16 in parental SC cells inducibly expressing mCherry owing to large tumor sizes (Fig. 8E,F). The tumors from parental SC cells with inducible mCherry reached the highest weight despite the shorter period of time. The SCpkn3^{-/-} cells expressing mCherry induced the smallest tumors among all groups. Re-expression of PKN3 WT, but not PKN3 mPR, in SCpkn3^{-/-} cells led to significant increase of tumors weight when compared to that for unmodified SCpkn3^{-/-} cells (Fig. 8C,D). Even though the tumors from SCpkn3^{-/-} cells re-expressing PKN3 mPR were removed 1 day later than those from SCpkn3^{-/-} re-expressing PKN3 WT, their statistical comparison (ANOVA on ranks, Tukey's *post hoc* test) yielded an almost significant P value of 0.059, indicating that PKN3 likely promotes tumor growth from SCpkn3^{-/-} cells and that the PKN3–p130Cas interaction may be important in this promotion.

We further analyzed individual tumors for the expression of mCherry as a reporter for Dox-induced expression in the tumor cells by dot blot analysis (Fig. S7C). Despite the comparable PKN3 mPR and

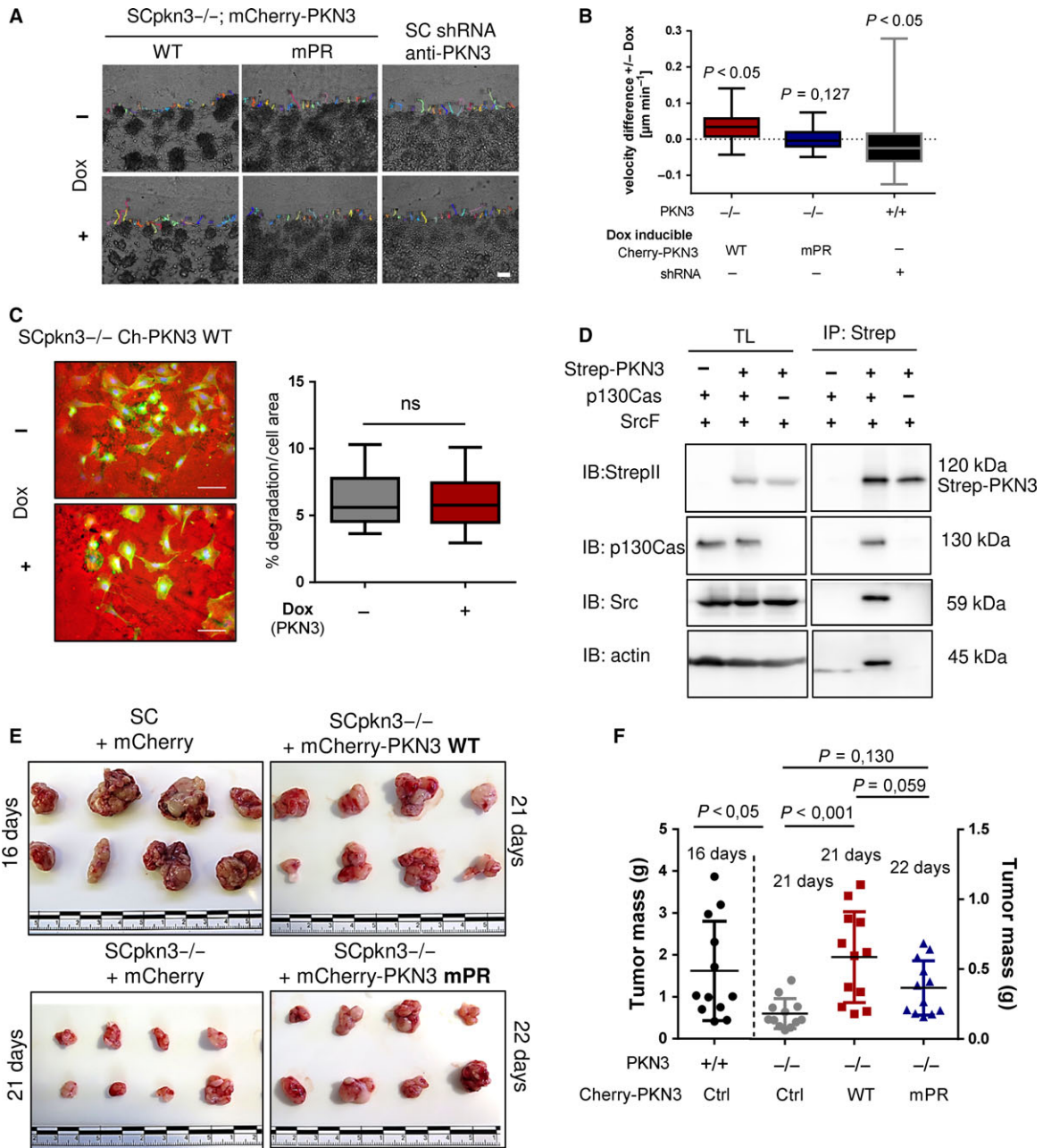


Fig. 8. PKN3 regulates cell migration in 3D environment of SrcF-transformed MEFs and tumor growth *in vivo* through interaction with p130Cas. (A) Representative tracking maps of SC or SCpkcn3^{-/-} cells stably expressing mCherry-PKN3 WT, mPR, or shRNA anti-PKN3 in Dox-dependent manner as indicated are shown (scale bar 100 μm). Cells migrated into collagen with or without Dox supplementation. (B) Quantification of cell velocity difference between induced and noninduced controls. Statistical significance was evaluated from 3 to 5 independent experiments by one-way ANOVA on ranks followed by Turkey *post hoc* test. (C) Gelatin degradation (Cy3-labeled) of SCpkcn3^{-/-} cells expressing Dox-inducible mCherry-PKN3. Representative images are shown (on the left). Scale bar represents 100 μm . Quantification calculated as % degraded area related to total cell area stained by phalloidin 488 (on the right). (D) Association of PKN3 with Src and Actin in p130Cas-dependent manner is shown by co-immunoprecipitations. SrcF-transformed cells with or without p130Cas were transfected by Strep-PKN3, and PKN3 was precipitated by Strep-Tactin[®] Superflow[®] resin followed by western blotting and detection by anti-StrepII antibody. Co-immunoprecipitated p130Cas, Src, and Actin were detected using appropriate antibodies (anti-p130Cas, anti-Src, anti-Actin). (E) Eight representative tumors of SC or SCpkcn3^{-/-} cells with Dox-induced mCherry, mCherry-PKN3, or mCherry-PKN3 mPR are shown with the same scale (units in cm). (F) Their respective quantification expressed as tumor mass weight at defined timescale as indicated. Statistics were evaluated by ANOVA on Ranks Dunn's Method. TL, total cell lysate; IP, immunoprecipitation; Ctrl, control sample prepared from SC cells.

WT protein level produced by Dox-induced cells *in vitro*, the majority of mCherry-PKN3 mPR-expressing tumors exhibited significantly increased mCherry signal compared to tumors with mCherry-PKN3 WT. This increase, however, did not lead to comparable tumor growth.

As p130Cas (Brábek *et al.*, 2005) as well as PKN3 (Unsal-Kacmaz *et al.*, 2012) expression is able to promote metastasis, we also evaluated the presence of lung metastases after 14 days postsurgery in animals injected with the parental SC cells, and after 21 days for all SCpkn3^{-/-} cells, as schematically represented in Fig. S7D. Metastases were clearly observed only in 3 out of 5 surviving mice injected with the parental SC cell line (Fig. S7E), suggesting that 21 days postsurgery (total 42 days) was not a sufficient time period for the formation of detectable metastases in mice injected with SCpkn3^{-/-} cells.

4. Discussion

In this study, we have, for the first time, shown and characterized PKN3–p130Cas interaction and provided new insight into the molecular mechanism of the regulation of tumor-promoting kinase PKN3 and p130Cas-mediated signaling. In particular, we demonstrated that PKN3–p130Cas interaction is necessary for PKN3 to promote malignant growth and invasiveness of SrcF-transformed MEFs. The interaction between mouse p130Cas and mouse PKN3 is mediated by binding of the p130Cas SH3 domain and PKN3 central polyproline region (P₅₀₀PPKPPRL; Fig. 1A–F). The dynamics of this interaction is potentially regulated similarly as that of other p130Cas SH3 ligands by Src-dependent phosphorylation of the p130Cas SH3 domain on Tyr12, which in its nonphosphorylated state contributes significantly to p130Cas SH3 ligand binding (Gemperle *et al.*, 2017). In addition, p130Cas–PKN3 binding is also regulated by the accessibility of the central polyproline region of PKN3 for the p130Cas binding since the introduction of the inactivating mutation into PKN3 kinase significantly decreased p130Cas–PKN3 interaction, presumably due to the closed conformation of PKN3 in the inactive state.

The PKN3–p130Cas interaction represents new crosstalk within PI3K–integrin signaling. p130Cas was previously shown to be in complex with PI3K to support anti-estrogenic drug-resistant cell growth (Cabodi *et al.*, 2004). The connection of PKN3 to integrin signaling was indicated by a study showing that PKN3 KO decreased chemotaxis of MEFs toward FN and caused a glycosylation defect of integrin β 1 and

integrin α 5 (Mukai *et al.*, 2016). Moreover, PKN3 promotes osteoclasts to resorb bone matrix via stimulation of integrin effector kinase–Src kinase (Uehara *et al.*, 2017). This effect was strongly dependent on the PKN3 polyproline region that we showed to be responsible for p130Cas binding. Here, we were able to demonstrate that the PKN3–Src association is indeed mediated by p130Cas (Fig. 8D).

PKN3 is the first kinase documented to phosphorylate p130Cas on Ser/Thr residues *in vitro* (Fig. 4E). Ser/Thr residues are abundantly present on p130Cas and yield a dynamic phosphorylation pattern (Makkinje *et al.*, 2009). One of these p130Cas residues, Ser432 (homologous to human Ser428), is highly phosphorylated in breast carcinoma tumors (Fig. 4D) and represents one of the major Ser/Thr phosphorylation sites in MEFs cultivated *in vitro* (Fig. 4F). Notably, some phosphoproteomic studies have shown that this phosphorylation is enriched in response to insulin, which is also a potent activator for PKN3 (PhosphoSite database, Leenders *et al.*, 2004), and correlates with PKN3 activity in breast carcinoma tumors (Fig. 4D). The effects of this phosphorylation as well as that of p130Cas in the SRD domain are still unknown, as p130Cas^{-/-} MEFs with reintroduced GFP-p130Cas 15AN increased cell growth and invasiveness similarly as GFP-p130Cas WT in a PKN3-dependent manner (Figs S3D and S4C,D). Further experiments with MDA-MB-231 cells showed that p130Cas migration pattern on SDS/PAGE, previously shown to be modulated by protein BCAR3 (Makkinje *et al.*, 2009), is not changed by PKN3 downregulation/upregulation (Fig. S5F and Fig. 7J). This suggests that although PKN3 kinase is able to phosphorylate p130Cas on Ser432 (Ser428) *in vitro* and its activity correlates with this phosphorylation in breast carcinomas, PKN3 is not responsible for this phosphorylation in cells cultivated on plastic.

We found PKN3 to colocalize with p130Cas in pro-invasive structures: lamellipodia of MEFs and podosome rosettes of Src-transformed MEFs (Fig. 2A,B). Notably, PKN3 was not detected at focal adhesions, which are highly redundant in terms of protein composition with podosome rosettes, whereas p130Cas is present in both structures. As PKN family kinases are implicated in cell migration, we investigated the role of PKN3 in cell migration and invasiveness. MEF migration as measured by wound healing assay (2D) was not affected by PKN3 overexpression (Fig. 6A,B). In contrast, we observed increased cell velocity in collagen (3D) upon induction of PKN3 expression, but not expression of a kinase inactive PKN3 variant (KD) or a PKN3 variant unable to bind p130Cas (mPR).

Moreover, the effect of PKN3 expression on migration in 3D was dependent on p130Cas expression (Figs 6C–G and 8A,B). Our results are consistent with independent studies wherein the invasiveness of SrcF-transformed MEFs through Matrigel was greatly decreased in the absence of p130Cas (Brábek *et al.*, 2005) and where MEF PKN3 KO cells exhibited lower migratory activity induced by various treatments than that of MEFs with endogenous PKN3 (Mukai *et al.*, 2016).

The role of PKN3 in the aggressiveness (malignant growth) of invasive breast cancer cell lines (MDA-MB-231) has already been demonstrated (Unsal-Kacmaz *et al.*, 2012). We have now verified these results and shown that PKN3-induced both proliferation in 2D and aggressive cell growth in 3D in p130Cas-dependent manner also in MDA-MB-231 cells (Fig. 7J–N and Fig. S5A,B). In contrast to fibroblasts, however, PKN3-induced expression did not increase MDA-MB-231 cell invasive migration in collagen (Fig. S5C,D). Stromal PKN3 has been demonstrated to promote metastasis formation of melanoma B16BL6 cells injected into mice (Mukai *et al.*, 2016), suggesting that cancer-associated fibroblast could lead invasion of cancer cells in PKN3-promoting manner.

Given the observation that disruption of actin-filaments interferes with PKN3 signaling (Fig. S6B,C) and that actin cytoskeleton remodeling protein p130Cas mediates interactions with actin and Src/PYK2 kinase which are necessary for PKN3 signaling in actin rings of osteoclasts (Fig. 8D) (Uehara *et al.*, 2017), we suggest that PKN3 affects cell growth (invasive migration) through intracellular local actin dynamics with the co-involvement of p130Cas. Indeed, it is well known that the actin cytoskeleton is a key regulator of cell proliferation (Heng and Koh, 2010). We plan to provide more detailed clarification of the mechanisms in future.

Furthermore, transformation of MEFs by a constitutive active Src led to an increase of PKN3 endogenous protein levels in cells grown on plastic, which was dependent on the presence of p130Cas (Fig. 7A and Fig. S7A). Similarly, PKN3 levels were shown to be elevated by its activators PI3K (Leenders *et al.*, 2004) and RhoA/C (Unsal-Kacmaz *et al.*, 2012), and by the oncogenic form of Ras (Leenders *et al.*, 2004). This suggests that PKN3 functions as an effector of various signal transduction pathways that mediate cell growth and transformation.

Several studies have presented evidence for the significant contribution of PKN3 and p130Cas to tumor growth as well as metastasis formation (Brábek *et al.*, 2005; Kang *et al.*, 2015; Leenders *et al.*, 2004; Tornillo *et al.*, 2014; Unsal-Kacmaz *et al.*, 2012). Our data support these results and furthermore suggest that binding

of PKN3 to p130Cas is important for PKN3-induced tumor growth. We hypothesize that targeting p130Cas, PKN3, and their co-operation may be exploited in cancer therapy and, based on our insight in PKN3 signaling in osteoclasts, potentially in pathophysiological signaling related to bone disease such as osteoporosis, rheumatoid arthritis, and periodontal disease as well. Moreover, a therapeutic agent that targets PKN3 by RNA interference (siRNA Atu027) has already completed Phase I clinical trials in a study with patients exhibiting different solid advanced and metastatic tumors, showing very promising results without any adverse effects (Schultheis *et al.*, 2014), further supporting the validity of this strategy.

5. Conclusion

In this study, we characterized PKN3 as a direct p130Cas binding protein using molecular, functional, and microscopic analyses *in vitro* and *in vivo*. Notably, we show that PKN3 phosphorylates p130Cas and colocalizes with p130Cas to pro-invasive cell structures and PKN3–p130Cas interaction is required for increased cell invasiveness and malignant growth. In summary, we suggest that aberrantly expressed PKN3 and p130Cas can cooperate in cancer progression and tumor growth and therefore may represent an attractive target for therapeutic intervention.

Acknowledgements

This work was funded by Czech Science Foundation grants 15-17419S and 15-07321S, by the Ministry of Education, Youth and Sports of CR within the LQ1604 National Sustainability Program II (Project BIOCEV-FAR), by the Charles University Grant Agency (224217), and in part by project ‘Center for Tumor Ecology – Research of the Cancer Microenvironment Supporting Cancer Growth and Spread’ (reg. no. CZ.02.1.01/0.0/0.0/16_019/0000785) supported by the Operational Programme Research, Development and Education. We acknowledge support by the MEYS CR (CZ.02.1.01/0.0/0.0/16_013/0001775 Czech-BioImaging) and support by the Imaging Methods Core Facility at BIOCEV Institution supported by the Czech-BioImaging large RI project (LM2015062 funded by MEYS CR) for their support with obtaining imaging data presented in this paper. We thank Marie Charvátová for technical help and L. Janečková for help with immunohistochemistry. We acknowledge Pfizer as the source of the materials and thank Dr Keziban Unsal-Kacmaz by providing the anti-phospho Thr849 PKN3 antibody (human Thr860) and plasmid

coding human PKN3. We would like to thank Editage (www.editage.com) for English language editing.

Conflict of interest

The authors declare no conflict of interest.

Author contributions

JG, DR, and JB conceived the design. JG, MD, and LK contributed to methodology. JG, MD, DR, and JB investigated the study. JB contributed to resources. JG wrote the original draft. JG, MD, DR, and JB wrote and reviewed the manuscript. JG performed the visualization. JB and DR performed the supervision of the article. JG, MD, JB, and DR funded the acquisition.

References

- Aleku M, Schulz P, Keil O, Santel A, Schaeper U, Dieckhoff B, Janke O, Endruschat J, Durieux B, Röder N *et al.* (2008) Atu027, a liposomal small interfering RNA formulation targeting protein kinase N3, inhibits cancer progression. *Cancer Res* **68**, 9788–9798.
- Astier A, Manié SN, Avraham H, Hirai H, Law SF, Zhang Y, Golemis EA, Fu Y, Druker BJ, Haghayeghi N *et al.* (1997) The related adhesion focal tyrosine kinase differentially phosphorylates p130Cas and the Cas-like protein, p105HEF1. *J Biol Chem* **272**, 19719–19724.
- Brábek J, Constancio SS, Shin NY, Pozzi A, Weaver AM and Hanks SK (2004) CAS promotes invasiveness of Src-transformed cells. *Oncogene* **23**, 7406–7415.
- Brábek J, Constancio SS, Siesser PF, Shin NY, Pozzi A and Hanks SK (2005) Crk-associated substrate tyrosine phosphorylation sites are critical for invasion and metastasis of Src-transformed cells. *Mol Cancer Res* **3**, 307–315.
- Braníš J, Pataki C, Spörrer M, Gerum RC, Mainka A, Cermak V, Goldmann WH, Fabry B, Brábek J and Rosel D (2017) The role of focal adhesion anchoring domains of CAS in mechanotransduction. *Sci Rep* **7**, 46233.
- Cabodi S, del Pilar Camacho-Leal M, Di Stefano P and Defilippi P (2010a) Integrin signalling adaptors: not only figurants in the cancer story. *Nat Rev Cancer* **10**, 858–870.
- Cabodi S, Moro L, Baj G, Smeriglio M, Di Stefano P, Gippone S, Surico N, Silengo L, Turco E, Tarone G *et al.* (2004) p130Cas interacts with estrogen receptor alpha and modulates non-genomic estrogen signaling in breast cancer cells. *J Cell Sci* **117**, 1603–1611.
- Cabodi S, Tinnirello A, Bisaro B, Tornillo G, del Pilar Camacho-Leal M, Forni G, Cojoca R, Iezzi M, Amici A, Montani M *et al.* (2010b) p130Cas is an essential transducer element in ErbB2 transformation. *FASEB J* **24**, 3796–3808.
- Cabodi S, Tinnirello A, Di Stefano P, Bisarò B, Ambrosino E, Castellano I, Sapino A, Arisio R, Cavallo F, Forni G *et al.* (2006) p130Cas as a new regulator of mammary epithelial cell proliferation, survival, and HER2-Neu oncogene-dependent breast tumorigenesis. *Cancer Res* **66**, 4672–4680.
- Collazos A, Michael N, Whelan RD, Kelly G, Mellor H, Pang LC, Totty N and Parker PJ (2011) Site recognition and substrate screens for PKN family proteins. *Biochem J* **438**, 535–543.
- Czauderna F, Santel A, Hinz M, Fechtner M, Durieux B, Fisch G, Leenders F, Arnold W, Giese K, Klippel A *et al.* (2003) Inducible shRNA expression for application in a prostate cancer mouse model. *Nucleic Acids Res* **31**, e127.
- Defilippi P, Di Stefano P and Cabodi S (2006) p130Cas: a versatile scaffold in signaling networks. *Trends Cell Biol* **16**, 257–263.
- Donato DM, Ryzhova LM, Meenderink LM, Kaverina I and Hanks SK (2010) Dynamics and mechanism of p130Cas localization to focal adhesions. *J Biol Chem* **285**, 20769–20779.
- Dorssers LC, Grebenchtchikov N, Brinkman A, Look MP, van Broekhoven SP, de Jong D, Peters HA, Portengen H, Meifer-van Gelder ME, Klijn JG *et al.* (2004) The prognostic value of BCAR1 in patients with primary breast cancer. *Clin Cancer Res* **10**, 6194–6202.
- Dorssers LC, Van der Flier S, Brinkman A, van Agthoven T, Veldscholte J, Berns EM, Klijn JG, Beex LV and Foekens JA (2001) Tamoxifen resistance in breast cancer: elucidating mechanisms. *Drugs* **61**, 1721–1733.
- Falk MD, Liu W, Bolaños B, Unsal-Kacmaz K, Klippel A, Grant S, Brooun A and Timofeevski S (2014) Enzyme kinetics and distinct modulation of the protein kinase N family of kinases by lipid activators and small molecule inhibitors. *Biosci Rep* **34**, 93–106.
- Fonseca PM, Shin NY, Brábek J, Rzhzova L, Wu J and Hanks SK (2004) Regulation and localization of CAS substrate domain tyrosine phosphorylation. *Cell Signal* **16**, 621–629.
- Fromont G and Cussenot O (2011) The integrin signalling adaptor p130CAS is also a key player in prostate cancer. *Nat Rev Cancer* **11**, 227.
- Fromont G, Vallancein G, Validire P, Levillain P and Cussenot O (2007) BCAR1 expression in prostate cancer: association with 16q23 LOH status, tumor progression and EGFR/KAI1 staining. *Prostate* **67**, 268–273.
- Gao J, Aksoy BA, Dogrusoz U, Dresdner G, Gross B, Sunner SO, Sun Y, Jacobsen A, Sinha R, Larsson E *et al.* (2013) Integrative analysis of complex cancer genomics and clinical profiles using the cBioPortal. *Sci Signal* **6**, pii.

- Garcia-Guzman M, Dolfi F, Russello M and Vuori K (1999) Cell adhesion regulates the interaction between the docking protein p130(Cas) and the 14-3-3 proteins. *J Biol Chem* **274**, 5762–5768.
- Gemperle J, Hexnerová R, Lepšík M, Tesina P, Dibus M, Novotný M, Brábek J, Veverka V and Rosel D (2017) Structural characterization of CAS SH3 domain selectivity and regulation reveals new CAS interaction partners. *Sci Rep* **7**, 8057.
- Hashimoto T, Mukai H, Kawamata T, Taniguchi T, Ono Y and Tanaka C (1998) Localization of PKN mRNA in the rat brain. *Brain Res Mol Brain Res* **59**, 143–153.
- Heng YW and Koh CG (2010) Actin cytoskeleton dynamics and the cell division cycle. *Int J Biochem Cell Biol* **42**, 1622–1633.
- Hivert V, Pierre J and Raingeaud J (2009) Phosphorylation of human enhancer of filamentation (HEF1) on serine 369 induces its proteasomal degradation. *Biochem Pharmacol* **78**, 1017–1025.
- Honda H, Oda H, Nakamoto T, Honda Z, Sakai R, Suzuki T, Saito T, Nakamura K, Nakao K, Ishikawa T *et al.* (1998) Cardiovascular anomaly, impaired actin bundling and resistance to Src-induced transformation in mice lacking p130Cas. *Nat Genet* **19**, 361–365.
- Janoštiak R, Brábek J, Auernheimer V, Tatárová Z, Lautscham LA, Dey T, Gemperle J, Merkel R, Goldmann WH, Fabry B *et al.* (2014) CAS directly interacts with vinculin to control mechanosensing and focal adhesion dynamics. *Cell Mol Life Sci* **71**, 727–744.
- Janoštiak R, Tolde O, Brůhová Z, Novotný M, Hanks SK, Rösel D and Brábek J (2011) Tyrosine phosphorylation within the SH3 domain regulates CAS subcellular localization, cell migration, and invasiveness. *Mol Biol Cell* **22**, 4256–4267.
- Kang H, Kim C, Lee H, Rho JG, Seo JW, Nam JW, Song WK, Nam SW, Kim W and Lee EK (2015) Downregulation of microRNA-362-3p and microRNA-329 promotes tumor progression in human breast cancer. *Cell Death Differ* **23**, 484–495.
- Lachmann S, Jevons A, De Rycker M, Cassamassima A, Radtke S, Collazos A and Parker PJ (2011) Regulatory domain selectivity in the cell-type specific PKN-dependence of cell migration. *PLoS One* **6**, e21732.
- Leenders F, Möpert K, Schmiedeknecht A, Santel A, Czauderna F, Aleku M, Penschuck S, Dames S, Dternberger M, Röhl T *et al.* (2004) KN3 is required for malignant prostate cell growth downstream of activated PI 3-kinase. *EMBO J* **23**, 3303–3313.
- Lim WG, Chen X, Liu JP, Tan BJ, Zhou S, Smith A, Lees N, Hou L, Gu F, Yu XY *et al.* (2008) The C-terminus of PRK2/PKN γ is required for optimal activation by RhoA in a GTP-dependent manner. *Arch Biochem Biophys* **479L**, 170–178.
- Makkinje A, Near RI, Infusini G, Vanden Borre P, Bloom A, Cai D, Costello CE and Lerner A (2009) AND-34/BCAR3 regulates adhesion-dependent p130Cas serine phosphorylation and breast cancer cell growth pattern. *Cell Signal* **21**, 1423–1435.
- Mellor H, Flynn P, Nobes CD, Hall A and Parker PJ (1998) PRK1 is targeted to endosomes by the small GTPase, RhoB. *J Biol Chem* **273**, 4811–4814.
- Möpert K, Löffler K, Röder N, Kaufmann J and Santel A (2012) Depletion of protein kinase N3 (PKN3) impairs actin and adherens junctions dynamics and attenuates endothelial cell activation. *Eur J Cell Biol* **91**, 694–705.
- Mukai H, Muramatsu A, Mashud R, Kubouchi K, Tsujimoto S, Hongu T, Kanaho Y, Tsubaki M, Nishida S, Shiol G *et al.* (2016) PKN3 is the major regulator of angiogenesis and tumor metastasis in mice. *Sci Rep* **6**, 18979.
- Mukai H and Ono Y (1994) A novel protein kinase with leucine zipper-like sequences: its catalytic domain is highly homologous to that of protein kinase C. *Biochem Biophys Res Commun* **199**, 897–904.
- Nagai Y, Osawa K, Fukushima H, Tamura Y, Aoki K, Ohya K, Yasuda H, Hikiji H, Takahashi M, Seta Y *et al.* (2013) p130Cas, Crk-associated substrate, plays important roles in osteoclastic bone resorption. *J Bone Miner Res* **28**, 2449–2462.
- Nick AM, Stone RL, Armaiz-Pena G, Ozpolat B, Tekedereli I, Graybill WS, Landen CN, Villares G, Vivas-Mejia P, Bottsford-Miller J *et al.* (2011) Silencing of p130cas in ovarian carcinoma: a novel mechanism for tumor cell death. *J Natl Cancer Inst* **103**, 1596–1612.
- Nikonova AS, Gaponova AV, Kudinov AE and Golemis EA (2014) CAS proteins in health and disease: an update. *IUBMB Life* **66**, 387–395.
- Oishi K, Mukai H, Shibata H, Takahashi M and Ona Y (1999) Identification and characterization of PKN β , a novel isoform of protein kinase PKN: expression and arachidonic acid dependency are different from those of PKN α . *Biochem Biophys Res Commun* **261**, 808–814.
- Piccinini F, Kiss A and Horvath P (2015) Cell Tracker (not only) for dummies. *Bioinformatics* **32**, 955–957.
- Pylayeva Y, Gillen KM, Gerald W, Beggs HE, Reichardt LF and Giancotti FG (2009) Ras- and PI3K-dependent breast tumorigenesis in mice and humans requires focal adhesion kinase signaling. *J Clin Invest* **119**, 252–266.
- Quilliam LA, Lambert QT, Mickelson-Young L, Westwick JK, Sparks AB, Kay BK, Jenkins NA, Gilbert DJ, Copeland NG and Der CJ (1996) Isolation of a NCK-associated kinase, PRK2, an SH3-binding protein and potential effector of Rho protein signaling. *J Biol Chem* **271**, 28772–28776.
- Ran FA, Hsu PD, Wright J, Agarwala V, Scott DA and Zhang F (2013) Genome engineering using the CRISPR-Cas9 system. *Nat Protoc* **8**, 2281–2308.

- Riedl J, Crevenna AH, Kessenbrock K, Yu JH, Neukirchen D, Bista M, Bradke F, Jenne D, Holak TA, Werb Z *et al.* (2008) Lifeact: a versatile marker to visualize F-actin. *Nat Methods* **5**, 605–607.
- Ruest PJ, Shin NY, Polte TR, Zhang X and Hanks SK (2001) Mechanisms of CAS substrate domain tyrosine phosphorylation by FAK and Src. *Mol Cell Biol* **21**, 7641–7652.
- Santel A, Aleku M, Röder N, Möpert K, Durieux B, Janke O, Keil O, Endruschat J, Dames S, Lange C *et al.* (2010) Atu027 prevents pulmonary metastasis in experimental and spontaneous mouse metastasis models. *Clin Cancer Res* **16**, 5469–5480.
- Schindelin J, Arganda-Carreras I, Frise E, Kaynig V, Longair M, Pietzsch T, Rueden C, Saalfeld S, Schmid B, Tinevez JY *et al.* (2012) Fiji: an open-source platform for biological-image analysis. *Nat Methods* **9**, 676–682.
- Schultheis B, Strumberg D, Santel A, Vank C, Gebhardt F, Keil O, Lange C, Giese K, Kaufmann J, Khan M *et al.* (2014) First-in-human phase I study of the liposomal RNA interference therapeutic Atu027 in patients with advanced solid tumors. *J Clin Oncol* **32**, 4141–4148.
- Strumberg D, Schultheis B, Traugott U, Vank C, Santel A, Keil O, Giese K, Kaufmann J and Dreves J (2012) Phase I clinical development of Atu027, a siRNA formulation targeting PKN3 in patients with advanced solid tumors. *Int J Clin Pharmacol Ther* **50**, 76–78.
- Ta HQ, Thomas KS, Schrecengost RS and Bouton AH (2008) A novel association between p130Cas and resistance to the chemotherapeutic drug adriamycin in human breast cancer cells. *Cancer Res* **68**, 8796–8804.
- Tarone G, Cirillo D, Giancotti FG, Cornoglio PM and Marchisio PC (1985) Rous sarcoma virus-transformed fibroblasts adhere primarily at discrete protrusions of the ventral membrane called podosomes. *Exp Cell Res* **159**, 141–157.
- Tazaki T, Miyazaki K, Hiyama E, Nakamoto T, Sakai R, Yamasaki N, Honda Z, Noda M, Miyasaka N, Sueda T *et al.* (2008) Functional analysis of Src homology 3-encoding exon (exon 2) of p130Cas in primary fibroblasts derived from exon 2-specific knockout mice. *Genes Cells* **13**, 145–157.
- Tikhmyanova N, Little JL and Golemis EA (2010) CAS proteins in normal and pathological cell growth control. *Cell Mol Life Sci* **67**, 1025–1048.
- Tornillo G, Defilippi P and Cabodi S (2014) Cas proteins: dodgy scaffolding in breast cancer. *Breast Cancer Res* **16**, 443.
- Uehara S, Udagawa N, Mukai H, Ishihara A, Maeda K, Yamashita T, Murakami K, Nishita M, Nakamura T, Kato S *et al.* (2017) Protein kinase N3 promotes bone resorption by osteoclasts in response to Wnt5a-Ror2 signaling. *Sci Signal* **10**, ean0023.
- Unsal-Kacmaz K, Ragunathan S, Rosfjord E, Dann S, Upešlaciš E, Grillo M, Hernandez R, Mack F and Klippel A (2012) The interaction of PKN3 with RhoC promotes malignant growth. *Mol Oncol* **6**, 284–298.
- Van Troys M, Masuzzo P, Huyck L, Bakkali K, Waterschoot D, Martens L and Ampe C (2018) Analysis of invasion dynamics of matrix-embedded cells in a multisample format. *Methods Mol Biol* **1749**, 79–117.
- Vincent S, Settleman J (1997) The PRK2 kinase is a potential effector target of both Rho and Rac GTPases and regulates actin cytoskeletal organization. *Mol Cell Biol* **17**, 2247–2256.
- Yamakita Y, Totsukawa G, Yamashiro S, Fry D, Zhang X, Hanks SK and Matsumura F (1999) Dissociation of FAK/p130(CAS)/c-Src complex during mitosis: role of mitosis-specific serine phosphorylation of FAK. *J Cell Biol* **144**, 315–324.

Supporting information

Additional supporting information may be found online in the Supporting Information section at the end of the article.

Fig. S1. PKN3 colocalizes with stress fibers; PKN3 activity.

Fig. S2. Co-expression of human p130Cas/BCAR1 and PKN3 in prostate and breast tumors; PKN3 and p130Cas phosphorylation.

Fig. S3. The influence of PKN3 and GFP-p130Cas variants expression on cell morphology and growth.

Fig. S4. PKN3 and signaling in MEFs; PKN3 dependent invasiveness is independent of phosphorylation in p130Cas SRD.

Fig. S5. The effect of p130Cas and PKN3 on cell growth and signaling in MDA-MB-231.

Fig. S6. The effect of different inhibitors on PKN3-induced growth of MDApkn3^{-/-} cells.

Fig. S7. Crosstalk of PKN3 with Src is p130Cas dependent; tumors and metastasis.

Table S1. geneArt sequences.

Table S2. Sequences of oligonucleotides (primers).

Movie S1. Colocalization of GFP-PKN3 WT and actin in lamellipodia of transfected MEF.

Movie S2. No colocalization of transfected GFP-PKN3 mPR with actin rich structures in lamellipodia of MEF.

Movie S3. Filopodia-like protrusions of MEFs transfected by GFP-PKN3 KD.

Movie S4. 3D cell-zone exclusion assay of p130Cas^{-/-} MEFs re-expressing p130Cas ± Dox.

Movie S5. 3D cell-zone exclusion assay of p130Cas^{-/-} MEFs ± Dox.